PHYSICAL REVIEW D **96,** 076001 (2017)

$B_c \to (J/\Psi,\eta_c)\tau\nu$ semileptonic decays within the standard model and beyond

Rupak Dutta[1,*] and Anupama Bhol[2,†]

[1]*National Institute of Technology Silchar, Silchar 788010, India*

[2]*C. V. Raman College of Engineering, Bhubaneswar, Odisha 752054, India*

(Received 25 April 2017; revised manuscript received 5 September 2017; published 2 October 2017)

Deviations from the standard model prediction have been observed not only in $b \to c$ charged current interactions but also in $b \to s$ flavor changing neutral current interactions. In particular, the deviation observed in the measured ratio of branching fractions $R_D = \mathcal{B}(B \to D\tau\nu)/\mathcal{B}(B \to Dl\nu)$ and $R_{D^*} = \mathcal{B}(B \to D^*\tau\nu)/\mathcal{B}(B \to D^*l\nu)$, where $l = (e,\mu)$, is more pronounced and the combined excess currently stands at a 3.9σ level. If it persists and is confirmed by future experiments, it would be a definite hint of new physics. In this context, we consider $B_c \to \eta_c l\nu$ and $B_c \to J/\Psi l\nu$ decays mediated via $b \to cl\nu$ charged current interactions and employ an effective theory approach to give a prediction on various observables such as the ratio of the branching ratio, tau polarization fraction, and forward-backward asymmetry for these decay modes.

DOI: 10.1103/PhysRevD.96.076001

I. INTRODUCTION

Although no direct evidence of new physics (NP) has been reported so far, there still exists some discrepancies with the standard model (SM) prediction. In particular, deviations from the SM expectation in both charged current $b \to c\tau\nu$ transitions as well as neutral current $b \to s\bar{l}l$ transitions have been observed in various measurements. The decays $B \to (D, D^*)\tau\nu$ and the lepton flavor universality ratios R_D and R_{D^*} have been studied by *BABAR* [1,2], BELLE [3–5], and LHCb [6] experiments. Various measurements of R_D and R_{D^*} are collected in Table I. The first unquenched lattice determination of the ratio of the branching ratio $R_D = 0.299 \pm 0.011$ [7] was reported by the FNAL/MILC Collaboration which is in excellent agreement with the value of $R_D = 0.300 \pm 0.008$ [8] reported by the HPQCD Collaboration. In Ref. [9], the authors obtain $R_D = 0.299 \pm 0.003$ by combining the two lattice calculations, with the experimental form factor of the $B \to Dl\nu$ from *BABAR* and BELLE. The result is compatible with the results above, but more accurate. The FLAG working group combines the two lattice calculations and reports the value of R_D to be 0.300 ± 0.008 [10]. The SM prediction for R_{D^*} is 0.252 ± 0.003 [11]. At present, the deviation of the measured values of R_D and R_{D^*} from the SM expectation is exceeded by 2.2σ and 3.4σ, respectively [12]. Considering the R_D-R_{D^*} correlation, the difference with the SM predictions currently stands at about 3.9σ [12]. For theoretical implications of these anomalies, we refer to Refs. [11,13–54] and references therein. Very recently, the first measurement of the tau polarization fraction $P_\tau^{D^*} = -0.44 \pm 0.47^{+0.20}_{-0.17}$ in the decay $B \to D^*\tau\nu$ was reported by BELLE [5].

The B_c meson, a pseudoscalar ground state composed of two heavy quarks b and c, first observed by the CDF Collaboration in $p\bar{p}$ collisions [55], has a promising prospect on the hadron colliders, as around 5×10^{10} B_c events per year are expected at LHC experiments [56,57]. Being composed of two heavy quarks, the B_c meson has the unique ability to decay via both the b and c quark. Although the b decays are cabbibo suppressed, the charm quark decays, however, are cabbibo favored decays as the Cabibbo-Kobayashi-Maskawa (CKM) matrix element $V_{cs} = 1$ is much larger than $V_{cb} = 0.04$. The estimates of the B_c total decay width indicate that the c quark transitions provide the dominant contribution while the b quark transitions and weak annihilation contribute less. The c quark decays provide around 70% to the total decay width of the B_c meson [56]. Although an indirect constraint can be imposed on various NP from the experimentally measured total decay width of B_c meson; however, measurements of various taunic decays of the B_c meson in the future will give direct access to the beyond the SM physics. The mean lifetime of the B_c meson $\tau_{B_c} = 0.52^{+0.18}_{-0.12}$ ps in the SM, calculated using operator product expansion and nonrelativistic QCD [58–60], is consistent with the measured mean lifetime, $\tau_{B_c} = 0.507(8)$ ps [61–63]. One can infer from this calculation that no more than 5% of the total

TABLE I. Current status of R_D and R_{D^*} [12].

Experiments	R_{D^*}	R_D
BABAR	$0.332 \pm 0.024 \pm 0.018$	$0.440 \pm 0.058 \pm 0.042$
BELLE	$0.293 \pm 0.038 \pm 0.015$	$0.375 \pm 0.064 \pm 0.026$
BELLE	$0.302 \pm 0.030 \pm 0.011$	
LHCb	$0.336 \pm 0.027 \pm 0.030$	
BELLE	$0.276 \pm 0.034^{+0.029}_{-0.026}$	
AVERAGE	$0.310 \pm 0.015 \pm 0.008$	$0.403 \pm 0.040 \pm 0.024$

*rupak@phy.nits.ac.in

†anupama.phy@gmail.com

decay width of the B_c meson can be explained by the semi (taunic) decays of the B_c meson. This was confirmed by various other SM calculations as well [64,65]. The constraint, however, can be relaxed up to around 30% depending on the value of the total decay width of the B_c meson that is used as input for the SM calculation of various partonic transitions.

The B_c meson and its decays have been widely studied in the literature [66–90]. The decays $B_c \to (J/\Psi, \eta_c) l\nu$ are mediated via $b \to c l\nu$ transitions and, in principle, NP effects might enter into these decay modes as well. The SM prediction of these decay modes are already studied by various authors [67–70,72,77,78,81,86–88]. Earlier discussions, however, have not looked into possible NP effects in these decay modes. In this study, we wish to study systematically the effect of NP couplings on various observables such as the ratio of branching ratios, forward-backward asymmetry, and τ polarization fraction pertaining to $B_c \to (J/\Psi, \eta_c)\tau\nu$ decays. To analyze the effect of NP couplings on various observables, we employ an effective theory approach for the $b \to c l\nu$ decay processes in the presence of NP that is valid at the renormalization scale $\mu = m_b$. We use 2σ constraints coming from the measured values of the ratio of the branching ratios R_D and R_{D^*} to explore various NP scenarios. The constraint coming from the total decay width of the B_c meson is also discussed in detail. We, however, do not use the constraint coming from the measured value of $P_\tau^{D^*}$ as the uncertainty associated with this observable reported by BELLE is rather large.

Our paper is organized as follows. In Sec. II, we introduce the most general effective Lagrangian for the $b \to c l\nu$ transition decays in the presence of NP. The two body $B_c \to \tau\nu$ and three body $B_c \to (J/\Psi, \eta_c) l\nu$ decay branching ratios are calculated and reported in Sec. II. Various observables such as the ratio of branching ratios, forward-backward asymmetries, and the τ polarization are defined. We report our analysis in Sec. III with a conclusion and summary in Sec. IV.

II. EFFECTIVE WEAK LAGRANGIAN, HELICITY AMPLITUDES, AND OBSERVABLES

A. Effective weak Lagrangian

We employ the effective field theory approach for the computation of various decay branching fractions in a model independent way. The most general effective weak Lagrangian at energy scale $\mu = m_b$ for the $b \to c l\nu$ transition decays can be expressed as [91,92]

$$\begin{aligned}\mathcal{L}_{\text{eff}} = -\frac{4G_F}{\sqrt{2}} V_{cb}\{&(1+V_L)\bar{l}_L\gamma_\mu\nu_L\bar{c}_L\gamma^\mu b_L + V_R\bar{l}_L\gamma_\mu\nu_L\bar{c}_R\gamma^\mu b_R + \tilde{V}_L\bar{l}_R\gamma_\mu\nu_R\bar{c}_L\gamma^\mu b_L \\ &+ \tilde{V}_R\bar{l}_R\gamma_\mu\nu_R\bar{c}_R\gamma^\mu b_R + S_L\bar{l}_R\nu_L\bar{c}_R b_L + S_R\bar{l}_R\nu_L\bar{c}_L b_R + \tilde{S}_L\bar{l}_L\nu_R\bar{c}_R b_L + \tilde{S}_R\bar{l}_L\nu_R\bar{c}_L b_R \\ &+ T_L\bar{l}_R\sigma_{\mu\nu}\nu_L\bar{c}_R\sigma^{\mu\nu} b_L + \tilde{T}_L\bar{l}_L\sigma_{\mu\nu}\nu_R\bar{c}_L\sigma^{\mu\nu} b_R\} + \text{H.c.}\end{aligned} \tag{1}$$

Neglecting the tensor NP couplings and following the same notation as in Ref. [36], the effective Lagrangian can be expressed as

$$\begin{aligned}\mathcal{L}_{\text{eff}} = -\frac{G_F}{\sqrt{2}} V_{cb}\{&G_V\bar{l}\gamma_\mu(1-\gamma_5)\nu_l\bar{c}\gamma^\mu b - G_A\bar{l}\gamma_\mu(1-\gamma_5)\nu_l\bar{c}\gamma^\mu\gamma_5 b + G_S\bar{l}(1-\gamma_5)\nu_l\bar{c}b \\ &- G_P\bar{l}(1-\gamma_5)\nu_l\bar{c}\gamma_5 b + \tilde{G}_V\bar{l}\gamma_\mu(1+\gamma_5)\nu_l\bar{c}\gamma^\mu b - \tilde{G}_A\bar{l}\gamma_\mu(1+\gamma_5)\nu_l\bar{c}\gamma^\mu\gamma_5 b \\ &+ \tilde{G}_S\bar{l}(1+\gamma_5)\nu_l\bar{c}b - \tilde{G}_P\bar{l}(1+\gamma_5)\nu_l\bar{c}\gamma_5 b\} + \text{H.c.},\end{aligned} \tag{2}$$

where

$$\begin{aligned}&G_V = 1 + V_L + V_R, \quad G_A = 1 + V_L - V_R, \quad G_S = S_L + S_R, \quad G_P = S_L - S_R \\ &\tilde{G}_V = \tilde{V}_L + \tilde{V}_R, \quad \tilde{G}_A = \tilde{V}_L - \tilde{V}_R, \quad \tilde{G}_S = \tilde{S}_L + \tilde{S}_R, \quad \tilde{G}_P = \tilde{S}_L - \tilde{S}_R.\end{aligned}$$

Here G_F is the Fermi coupling constant and V_{cb} is the CKM matrix element. The new vector and scalar NP interactions that involve left-handed neutrinos are denoted by $V_{L,R}$ and $S_{L,R}$ NP couplings. Similarly for the right-handed neutrinos the NP interactions are denoted by $\tilde{V}_{L,R}$ and $\tilde{S}_{L,R}$ NP couplings, respectively. All these NP couplings are defined at the renormalization scale, $\mu = m_b$. In the SM, all the NP couplings will be zero leading to $G_{V,A} = 1$, $G_{S,P} = 0$ and $\tilde{G}_{V,A,S,P} = 0$.

B. Helicity amplitudes and observables

We follow Refs. [93,94] to calculate the various helicity amplitudes for a B_q meson decaying to a pseudoscalar or to a vector meson along with a charged lepton and an antineutrino in the final state. Again, in order to calculate the partial decay width of $B_q \to l\nu$ and the differential decay rate of three body $B_q \to (P,V)l\nu$ decays, we need information on various nonperturbative hadronic matrix elements which are parametrized in terms of B_q meson decay constants and $B_q \to (P,V)$ transition form factors. We refer to Refs. [36,86] for a more detailed discussion.

In the presence of NP, the partial decay width of $B_q \to l\nu$ and differential decay width of three body $B_q \to (P,V)l\nu$ decays, where $P(V)$ stands for a pseudoscalar(vector) meson, can be expressed as [36]

$$\Gamma(B_q \to l\nu) = \frac{G_F^2|V_{cb}|^2}{8\pi} f_B^2 m_l^2 m_{B_q}\left(1-\frac{m_l^2}{m_{B_q}^2}\right)^2\left\{\left[G_A - \frac{m_{B_q}^2}{m_l(m_b(\mu)+m_c(\mu))}G_P\right]^2 + \left[\tilde{G}_A - \frac{m_{B_q}^2}{m_l(m_b(\mu)+m_c(\mu))}\tilde{G}_P\right]^2\right\}, \tag{3}$$

$$\frac{d\Gamma^P}{dq^2} = \frac{8N|\vec{p}_P|}{3}\left\{H_0^2(G_V^2+\tilde{G}_V^2)\left(1+\frac{m_l^2}{2q^2}\right) + \frac{3m_l^2}{2q^2}\left[\left(H_t G_V + \frac{\sqrt{q^2}}{m_l}H_S G_S\right)^2 + \left(H_t\tilde{G}_V + \frac{\sqrt{q^2}}{m_l}H_S\tilde{G}_S\right)^2\right]\right\} \tag{4}$$

and

$$\frac{d\Gamma^V}{dq^2} = \frac{8N|\vec{p}_V|}{3}\left\{\mathcal{A}_{AV}^2 + \frac{m_l^2}{2q^2}[\mathcal{A}_{AV}^2 + 3\mathcal{A}_{tP}^2] + \tilde{\mathcal{A}}_{AV}^2 + \frac{m_l^2}{2q^2}[\tilde{\mathcal{A}}_{AV}^2 + 3\tilde{\mathcal{A}}_{tP}^2]\right\}, \tag{5}$$

where

$$N = \frac{G_F^2|V_{cb}|^2 q^2}{256\pi^3 m_{B_q}^2}\left(1-\frac{m_l^2}{q^2}\right)^2, \qquad H_0 = \frac{2m_{B_q}|\vec{p}_P|}{\sqrt{q^2}}F_+(q^2)$$
$$H_t = \frac{m_{B_q}^2 - m_P^2}{\sqrt{q^2}}F_0(q^2), \qquad H_S = \frac{m_{B_q}^2 - m_P^2}{m_b(\mu)-m_c(\mu)}F_0(q^2),$$
$$\mathcal{A}_{AV}^2 = \mathcal{A}_0^2 G_A^2 + \mathcal{A}_\parallel^2 G_A^2 + \mathcal{A}_\perp^2 G_V^2, \qquad \tilde{\mathcal{A}}_{AV}^2 = \mathcal{A}_0^2\tilde{G}_A^2 + \mathcal{A}_\parallel^2\tilde{G}_A^2 + \mathcal{A}_\perp^2\tilde{G}_V^2,$$
$$\mathcal{A}_{tP} = \mathcal{A}_t G_A + \frac{\sqrt{q^2}}{m_l}\mathcal{A}_P G_P, \qquad \tilde{\mathcal{A}}_{tP} = \mathcal{A}_t\tilde{G}_A + \frac{\sqrt{q^2}}{m_l}\mathcal{A}_P\tilde{G}_P \tag{6}$$

and

$$\mathcal{A}_0 = \frac{1}{2m_V\sqrt{q^2}}\left[(m_{B_q}^2 - m_V^2 - q^2)(m_{B_q}+m_V)A_1(q^2) - \frac{4M_B^2|\vec{p}_V|^2}{m_{B_q}+m_V}A_2(q^2)\right],$$
$$\mathcal{A}_\parallel = \frac{2(m_{B_q}+m_V)A_1(q^2)}{\sqrt{2}}, \qquad \mathcal{A}_\perp = -\frac{4m_{B_q}V(q^2)|\vec{p}_V|}{\sqrt{2}(m_{B_q}+m_V)},$$
$$\mathcal{A}_t = \frac{2m_{B_q}|\vec{p}_V|A_0(q^2)}{\sqrt{q^2}}, \qquad \mathcal{A}_P = -\frac{2m_{B_q}|\vec{p}_V|A_0(q^2)}{(m_b(\mu)+m_c(\mu))}. \tag{7}$$

Here $|\vec{p}_{P(V)}| = \sqrt{\lambda(m_{B_q}^2, m_{P(V)}^2, q^2)}/2m_{B_q}$ is the three-momentum vector of the outgoing meson and $\lambda(a,b,c) = a^2+b^2+c^2-2(ab+bc+ca)$.

We define several observables such as the ratio of branching ratios and the tau polarization fraction for various semileptonic $b \to c$ transition decays. Those are

$$R_M = \frac{\mathcal{B}(B_q \to M\tau\nu)}{\mathcal{B}(B_q \to Ml\nu)}, \qquad P_\tau^M = \frac{\Gamma^M(+) - \Gamma^M(-)}{\Gamma^M(+) + \Gamma^M(-)}, \quad (8)$$

where, l is either an electron or a muon and B_q is either a B meson or a B_c meson. Similarly, M refers to the outgoing pseudoscalar or vector meson. Again, $\Gamma(+)$ and $\Gamma(-)$ denote the decay widths of positive and negative helicity τ leptons, respectively. We also construct various q^2 dependent observables such as differential branching fractions [DBR(q^2)], the ratio of branching fractions $R(q^2)$, forward-backward asymmetry parameter $A^{FB}(q^2)$, and the τ polarization parameter $P_\tau(q^2)$ for the $B_c \to (\eta_c, J/\Psi)\tau\nu$ decays such that

$$\mathrm{DBR}(q^2) = \left(\frac{d\Gamma}{dq^2}\right)/\Gamma_{\mathrm{tot}}, \qquad R_M(q^2) = \frac{\mathrm{DBR}(q^2)(B_q \to M\tau\nu)}{\mathrm{DBR}(q^2)(B_q \to Ml\nu)}$$
$$A_M^{FB}(q^2) = \frac{(\int_{-1}^{0} - \int_{0}^{1}) d\cos\theta_l \frac{d\Gamma^M}{dq^2 d\cos\theta_l}}{\frac{d\Gamma^M}{dq^2}}, \qquad P_\tau^M(q^2) = \frac{d\Gamma^M(+)/dq^2 - d\Gamma^M(-)/dq^2}{d\Gamma^M(+)/dq^2 + d\Gamma^M(-)/dq^2}, \quad (9)$$

where $d\Gamma^M(+)/dq^2$ and $d\Gamma^M(-)/dq^2$ denote the differential branching ratio of positive and negative helicity τ leptons, respectively. Here M represents the outgoing pseudoscalar (P) or vector (V) meson.

In the presence of various NP couplings, $d\Gamma^P(+)/dq^2$, $d\Gamma^P(-)/dq^2$, and the forward-backward asymmetry parameter $A_P^{FB}(q^2)$ for $B_q \to Pl\nu$, decays can be written as

$$d\Gamma^P(+)/dq^2 = \frac{8N|\vec{p}_P|}{3}\left\{H_0^2\tilde{G}_V^2 + \frac{m_l^2}{2q^2}\left[H_0^2 G_V^2 + 3\left(H_t G_V + \frac{\sqrt{q^2}}{m_l} H_S G_S\right)^2\right]\right\},$$
$$d\Gamma^P(-)/dq^2 = \frac{8N|\vec{p}_P|}{3}\left\{H_0^2 G_V^2 + \frac{m_l^2}{2q^2}\left[H_0^2\tilde{G}_V^2 + 3\left(H_t \tilde{G}_V + \frac{\sqrt{q^2}}{m_l} H_S \tilde{G}_S\right)^2\right]\right\},$$
$$A_P^{FB}(q^2) = \frac{3m_l^2}{2q^2}\frac{H_0 G_V(H_t G_V + \frac{\sqrt{q^2}}{m_l} H_S G_S) + H_0\tilde{G}_V(H_t\tilde{G}_V + \frac{\sqrt{q^2}}{m_l} H_S\tilde{G}_S)}{H_0^2(G_V^2 + \tilde{G}_V^2)(1 + \frac{m_l^2}{2q^2}) + \frac{3m_l^2}{2q^2}[(H_t G_V + \frac{\sqrt{q^2}}{m_l} H_S G_S)^2 + (H_t\tilde{G}_V + \frac{\sqrt{q^2}}{m_l} H_S\tilde{G}_S)^2]}. \quad (10)$$

Similarly, for $B_q \to Vl\nu$ decay mode, the explicit expressions for the differential branching ratio of positive and negative helicity τ leptons and the forward-backward asymmetry parameter are

$$d\Gamma^V(+)/dq^2 = \frac{8N|\vec{p}_V|}{3}\left\{\tilde{\mathcal{A}}_{AV}^2 + \frac{m_l^2}{2q^2}[\mathcal{A}_{AV}^2 + 3\mathcal{A}_{tP}^2]\right\},$$
$$d\Gamma^V(-)/dq^2 = \frac{8N|\vec{p}_V|}{3}\left\{\mathcal{A}_{AV}^2 + \frac{m_l^2}{2q^2}[\tilde{\mathcal{A}}_{AV}^2 + 3\tilde{\mathcal{A}}_{tP}^2]\right\},$$
$$A_V^{FB}(q^2) = \frac{3}{2}\frac{\mathcal{A}_\parallel\mathcal{A}_\perp(G_A G_V - \tilde{G}_A\tilde{G}_V) + \frac{m_l^2}{q^2}\left\{\mathcal{A}_0 G_A\left[\mathcal{A}_t G_A + \frac{\sqrt{q^2}}{m_l}\mathcal{A}_P G_P\right] + \mathcal{A}_0\tilde{G}_A\left[\mathcal{A}_t\tilde{G}_A + \frac{\sqrt{q^2}}{m_l}\mathcal{A}_P\tilde{G}_P\right]\right\}}{\mathcal{A}_{AV}^2 + \frac{m_l^2}{2q^2}[\mathcal{A}_{AV}^2 + 3\mathcal{A}_{tP}^2] + \tilde{\mathcal{A}}_{AV}^2 + \frac{m_l^2}{2q^2}[\tilde{\mathcal{A}}_{AV}^2 + 3\tilde{\mathcal{A}}_{tP}^2]}. \quad (11)$$

It is worth mentioning that for $B_q \to P\tau\nu$ decays, the tau polarization fraction does not depend on $V_{L,R}$ NP couplings if we assume that the NP effect is coming from new vector interactions $V_{L,R}$ only. Similarly, although the forward-backward asymmetry parameter does depend on all the NP couplings for $B_q \to V\tau\nu$ decays, it does not depend on $V_{L,R}$ and $\tilde{V}_{L,R}$ NP couplings for the $B_q \to P\tau\nu$ decays if we assume that only vector-type NP couplings contribute to these decay modes. The dependency gets canceled in the ratio. The tau polarization fraction and the forward-backward asymmetry parameter can, in principle, provide useful information regarding the various Lorentz structures of beyond the SM physics. We now proceed to discuss the results of our analysis.

III. NUMERICAL RESULTS AND DISCUSSIONS

A. Input parameters

We first report in Table II all the relevant input parameters that are used for our numerical estimates. For the quark, lepton, and meson masses, we use the most recent values reported in Ref. [61]. Similarly, for the mean lifetime of B^- and B_c mesons, we use the values reported in Ref. [61]. We use Ref. [95] for the B_c meson decay constant. The mass and decay constant reported in Table II are in GeV units, whereas, the mean lifetime of B^- and B_c meson are in seconds. The uncertainty associated with f_{B_c} and V_{cb} are indicated by the number in parentheses. The errors in all the other input parameters are unimportant for us and hence not included in Table II.

For the $B_c \to \eta_c$ and $B_c \to J/\Psi$ hadronic form factors, we follow Ref. [86]. The relevant formula for $F_0(q^2)$, $F_+(q^2)$, $V(q^2)$, $A_0(q^2)$, $A_1(q^2)$, and $A_2(q^2)$ pertinent for our discussion, taken from Ref. [86] is

$$F(q^2) = F(0)\exp[aq^2 + b(q^2)^2], \tag{12}$$

where F stands for the form factors F_0, F_+, V, A_0, A_1, and A_2 and a, b are the fitted parameters. The numerical values of $B_c \to \eta_c$ and $B_c \to J/\Psi$ form factors at $q^2 = 0$ and their fitted parameters a and b, calculated in the perturbative QCD (PQCD) approach, collected from Ref. [86], are listed in Table III. For our numerical analysis, we added the errors in quadrature. We also report the most important experimental input parameters R_D and R_{D^*} with their uncertainties measured by *BABAR*, BELLE, and LHCb in Table I. We use the average values of R_D and R_{D^*} for our analysis. In our analysis, we added the statistical and systematic uncertainties in quadrature. It may be noted that although there may be issues with the theoretical SM prediction due to various B_c meson form factors, we try to explore various NP effects nevertheless. A preliminary lattice QCD result for semileptonic form factors of the $B_c \to \eta_c l\nu$ and $B_c \to J/\Psi l\nu$ decays has been reported in Ref. [96].

B. Numerical analyses

The SM branching ratios, ratio of branching ratios, and the tau polarization fraction for all the relevant decay modes are presented in Table IV. We find the branching ratios of $B_c \to \eta_c\tau\nu$ and $B_c \to J/\Psi\tau\nu$ decays to be of the order of 10^{-3} which is quite similar to the values reported in Ref. [86]. Similarly, the branching ratio of $B_c \to \tau\nu$ is found to be of the order of 2%. The values of the ratio of branching ratios R_{η_c} and $R_{J/\Psi}$ are quite similar to the values reported in Ref. [86]. We also give the first prediction of the tau polarization fraction $P_\tau^{\eta_c}$ and $P_\tau^{J/\Psi}$ for the $B_c \to \eta_c\tau\nu$ and $B_c \to J/\Psi\tau\nu$ decay modes.

TABLE II. Theory input parameters.

$m_b(m_b)$	4.18	$m_{J/\Psi}$	3.0969	$m_{D^{*0}}$	2.00685
$m_c(m_b)$	0.91	m_{η_c}	2.9834	τ_{B^-}	1.638×10^{-12}
m_e	$0.510998928 \times 10^{-3}$	m_{B^-}	5.27931	τ_{B_c}	0.507×10^{-12}
m_μ	0.1056583715	m_{B_c}	6.2751	f_{B_c}	0.434(0.015)
m_τ	1.77682	m_{D^0}	1.86483	V_{cb}	0.0409(0.0011)

TABLE III. $B_c \to \eta_c$ and $B_c \to J/\Psi$ form factors at $q^2 = 0$ taken from Ref. [86].

Form Factors	F_0	a	b	Form Factors	F_0	a	b
$F_0^{B_c\to\eta_c}$	$0.48 \pm 0.06 \pm 0.01$	0.037	0.0007	$A_0^{B_c\to J/\Psi}$	$0.52 \pm 0.02 \pm 0.01$	0.047	0.0017
$F_+^{B_c\to\eta_c}$	$0.48 \pm 0.06 \pm 0.01$	0.055	0.0014	$A_1^{B_c\to J/\Psi}$	$0.46 \pm 0.02 \pm 0.01$	0.038	0.0015
$V^{B_c\to J/\Psi}$	$0.42 \pm 0.01 \pm 0.01$	0.065	0.0015	$A_2^{B_c\to J/\Psi}$	$0.64 \pm 0.02 \pm 0.01$	0.064	0.0041

TABLE IV. SM prediction of various observables.

Observables	Central Value	1σ Range	Observables	Central Value	1σ Range
$\mathcal{B}(B_c \to \tau\nu) \times 10^2$	2.20	[1.95, 2.48]	R_{η_c}	0.308	[0.235, 0.429]
$\mathcal{B}(B_c \to \eta_c l\nu) \times 10^3$	4.85	[3.50, 6.49]	$R_{J/\Psi}$	0.289	[0.279, 0.301]
$\mathcal{B}(B_c \to \eta_c\tau\nu) \times 10^3$	1.49	[1.09, 1.99]	$P_\tau^{\eta_c}$	0.345	[0.141, 0.530]
$\mathcal{B}(B_c \to J/\Psi l\nu) \times 10^3$	11.36	[9.44, 13.53]	$P_\tau^{J/\Psi}$	−0.465	[−0.433, −0.492]
$\mathcal{B}(B_c \to J/\Psi\tau\nu) \times 10^3$	3.29	[2.80, 3.83]	P_τ^D	0.336	[0.334, 0.338]
			$P_\tau^{D^*}$	−0.505	[−0.475, −0.532]

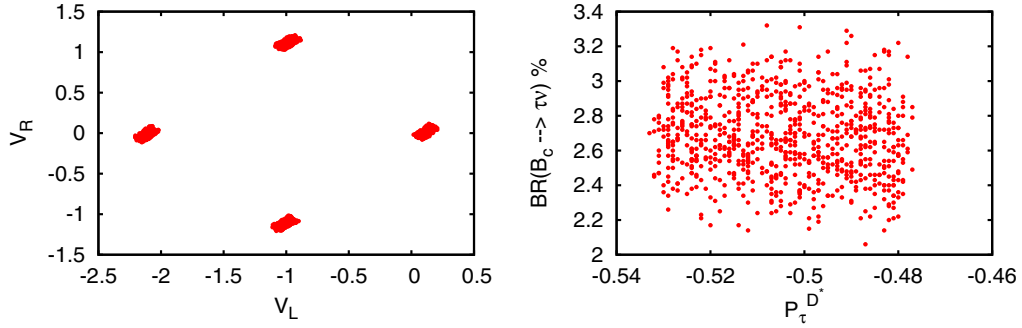

FIG. 1. Allowed ranges of V_L and V_R NP couplings are shown in the left panel once the 2σ constraint coming from the measured values of the ratio of branching ratios R_D and R_{D^*} is imposed. We show in the right panel the allowed ranges in $\mathcal{B}(B_c \to \tau\nu)$ and $P_\tau^{D^*}$ in the presence of these NP couplings.

Uncertainties in each observable may come from mainly two different sources: first it may come from not very well-known input parameters such as the CKM matrix elements and second, it may come from the hadronic input parameters such as meson to meson form factors and meson decay constants. To see the effect of the above mentioned uncertainties on various observables, we perform a random scan of all the input parameters such as the CKM matrix element, form factors, and decay constants within 1σ of their central values. The central values of all the observables obtained using the central values of all the input parameters and the 1σ range obtained from our random scan are reported in Table IV.

Now, let us provide an estimation of the expected number of events at the LHCb for $B_c \to (J/\Psi, \eta_c)\tau\nu$ decay modes. The number of expected events at the LHCb depends on various factors such as the production cross section of the B_c meson inside the LHCb geometrical acceptance, estimated branching ratio of the process in consideration, detection efficiency of the LHCb detector, and integrated luminosity. Although the production cross section of the B_c meson has not been measured yet, a rough estimate would give $\sigma(B_c) = 160$ nb at the center of mass energy of 14 TeV. Integrated luminosities of the order of 40–50 fb^{-1} are expected in LHC Run3 [97]. Again, precise computation of the detection efficiency can only be done by the experimental collaboration since it depends on various factors such as reconstruction, selection, trigger, and particle misidentification efficiencies. The LHCb Collaboration has measured the detection efficiency of the $B_c^+ \to J/\Psi\pi^+$ decay mode to be 6% [98]. Based on the study of some B_c decays by the LHCb, we assume a value of detection efficiency of around 1% for $B_c \to (J/\Psi, \eta_c)\tau\nu$ decays. Considering all the above assumptions, we estimate the total number of expected events to be observed in the LHCb experiment for the $B_c \to (J/\Psi, \eta_c)\tau\nu$ decays to be of $\mathcal{O}(10^4$–$10^5)$. Moreover, a more precise value of the production cross section will be known as the LHCb will perform a direct measurement of the production cross section of the B_c meson at the center of mass energy of 14 TeV. In any case, values of branching fractions of the $\mathcal{O}(10^{-4}$–$10^{-3})$ might be within the experimental sensitivity of the LHCb because of the large number of B_c events per year that is expected at LHC experiments. This is, however, just a naive estimate. Exact realistic limits can only be determined after incorporating the detection and reconstruction efficiencies of all the final particles.

We wish to determine the NP effect on each observable in a model independent way. We assume four different NP scenarios. All the NP couplings are assumed to be real for our analysis. Again, we consider that NP affects the third generation leptons only. The allowed NP parameter space is obtained by imposing a 2σ constraint coming from the measured values of the ratio of branching ratios R_D and R_{D^*}. This automatically guarantees that the resulting NP parameter space simultaneously explains the anomalies persisted in R_D and R_{D^*}. Now we proceed to discuss various NP scenarios.

1. Scenario I: Only V_L and V_R NP couplings

In this scenario, we have considered the effect of only V_L and V_R type NP couplings on various observables. In the left panel of Fig. 1, we show the allowed range of new

TABLE V. Allowed ranges of various observables in the presence of V_L and V_R NP couplings.

Observables	Range	Observables	Range	Observables	Range
$\mathcal{B}(B_c \to \tau\nu) \times 10^2$	[2.06, 3.32]	R_{η_c}	[0.240, 0.658]	$P_\tau^{J/\Psi}$	$[-0.435, -0.491]$
$\mathcal{B}(B_c \to \eta_c\tau\nu) \times 10^3$	[1.14, 2.97]	$R_{J/\Psi}$	[0.300, 0.413]	P_τ^{D}	[0.334, 0.338]
$\mathcal{B}(B_c \to J/\Psi\tau\nu) \times 10^3$	[3.12, 5.09]	$P_\tau^{\eta_c}$	[0.141, 0.530]	$P_\tau^{D^*}$	$[-0.477, -0.533]$

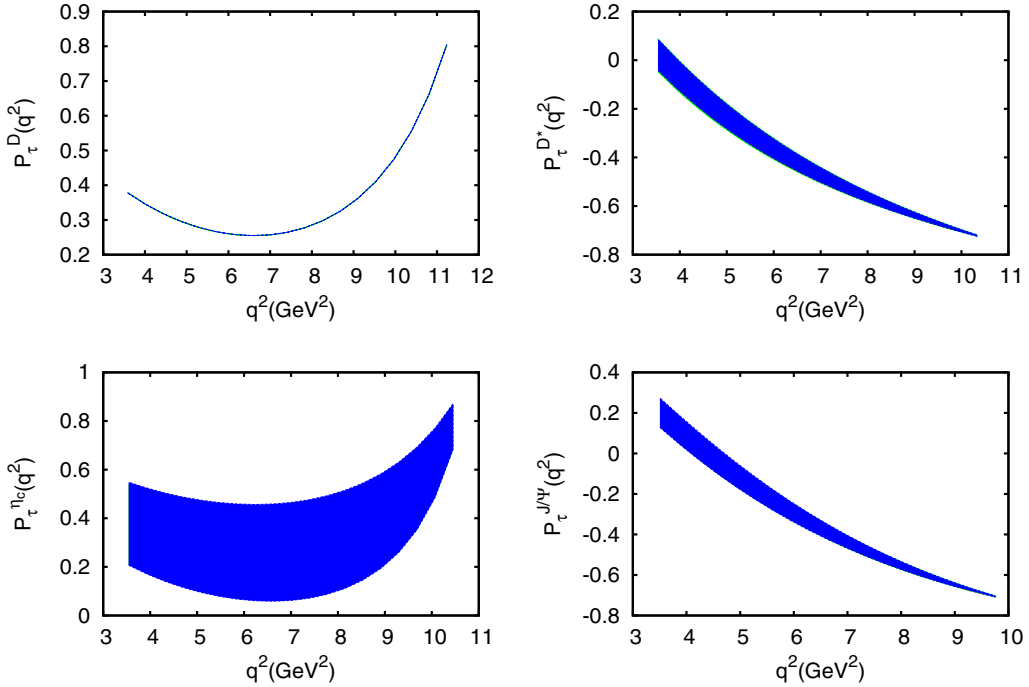

FIG. 2. Range in $P_\tau(q^2)$ for the $B \to (D, D^*)\tau\nu$ (upper panel) and $B_c \to (\eta_c, J/\Psi)\tau\nu$ (lower panel) decays. The allowed range in each observable is shown in the light (green) band once the NP couplings (V_L, V_R) are varied within the allowed ranges shown in the left panel of Fig. 1. We show in the dark (blue) band the corresponding SM prediction. The light (green) band overlaps with the dark (blue) band as we do not observe any deviation from the SM prediction.

vector couplings V_L and V_R that satisfies the 2σ experimental constraint coming from R_D and R_{D^*}. The range of each observable for V_L and V_R type NP couplings is tabulated in Table V. We also show in the right panel of Fig. 1 the allowed ranges of $\mathcal{B}(B_c \to \tau\nu)$ and the tau polarization fraction $P_\tau^{D^*}$. We want to emphasize that the central value of $P_\tau^{D^*}$ reported by BELLE lies outside the allowed range of $P_\tau^{D^*}$ obtained in this scenario. However, the measured 1σ range of the observable $P_\tau^{D^*}$ does overlap with the allowed range. Again, the uncertainty associated with the measured value of $P_\tau^{D^*}$ is rather large. The allowed range of $\mathcal{B}(B_c \to \tau\nu)$ is also compatible with the total decay width of the B_c meson. As expected, the tau polarization fraction pertaining to $B \to D\tau\nu$ and $B_c \to \eta_c\tau\nu$ decays does not vary at all as the NP effects coming from V_L and V_R couplings cancel in the ratios.

In Fig. 2, we show the effect of new vector couplings V_L and V_R on τ polarization parameter $P_\tau(q^2)$ for $B \to (D, D^*)\tau\nu$ and $B_c \to (\eta_c, J/\Psi)\tau\nu$ decays. We show in a dark (blue) band the SM range and show in a light (green) band the allowed range of each observable once the NP couplings V_L and V_R are switched on. It is observed that the new vector couplings do not affect $P_\tau(q^2)$. It is expected for the $B \to D\tau\nu$ and $B_c \to \eta_c\tau\nu$ decays as the NP dependency cancels in the ratio since the positive and negative τ helicity differential branching ratios $d\Gamma(\pm)/dq^2$ depend on G_V couplings only. It is, however, not true for the $B \to D^*\tau\nu$ and $B_c \to J/\Psi\tau\nu$ decays as the differential branching ratio depends on both G_V and G_A couplings. Although the NP dependency does not cancel in the τ polarization parameters $P_\tau^{D^*}$ and $P_\tau^{J/\Psi}$, they are indistinguishable from the SM prediction. It can be very well understood from the allowed ranges of V_L and V_R of Fig. 1. Again, it should be noted that although there is no zero crossing in the τ polarization parameters P_τ^D and $P_\tau^{\eta_c}$, there is zero crossing in $P_\tau^{D^*}$ and $P_\tau^{J/\Psi}$ at $q^2 = 3.9$ GeV^2 and $q^2 = 4.2$ GeV^2, respectively.

In Fig. 3, we show the effect of V_L and V_R NP couplings on various other observables such as the ratio of the branching ratio $R(q^2)$, the forward-backward asymmetry $A^{FB}(q^2)$, and the differential branching ratio $\mathrm{DBR}(q^2)$ as a function of q^2 for the $B_c \to \eta_c\tau\nu$ and $B_c \to J/\Psi\tau\nu$ decays. We show in dark (blue) band the SM range and show in light (green) band the allowed range of each observable once the NP couplings V_L and V_R are switched on. We see significant deviation from the SM prediction of all the observables. In the presence of V_L and V_R NP couplings, the differential branching ratio (DBR) and the ratio of the branching ratio for the $B_c \to \eta_c\tau\nu$ decays depend on G_V couplings only and are proportional to G_V^2. For the $B_c \to J/\Psi\tau\nu$ decays, the differential branching ratio and ratio of branching ratio depend not only on G_V but also on G_A couplings as well and they are proportional to G_V^2 and G_A^2. The forward-backward asymmetry parameter, $A^{FB}(q^2)$, does not vary with the NP couplings V_L and V_R for the

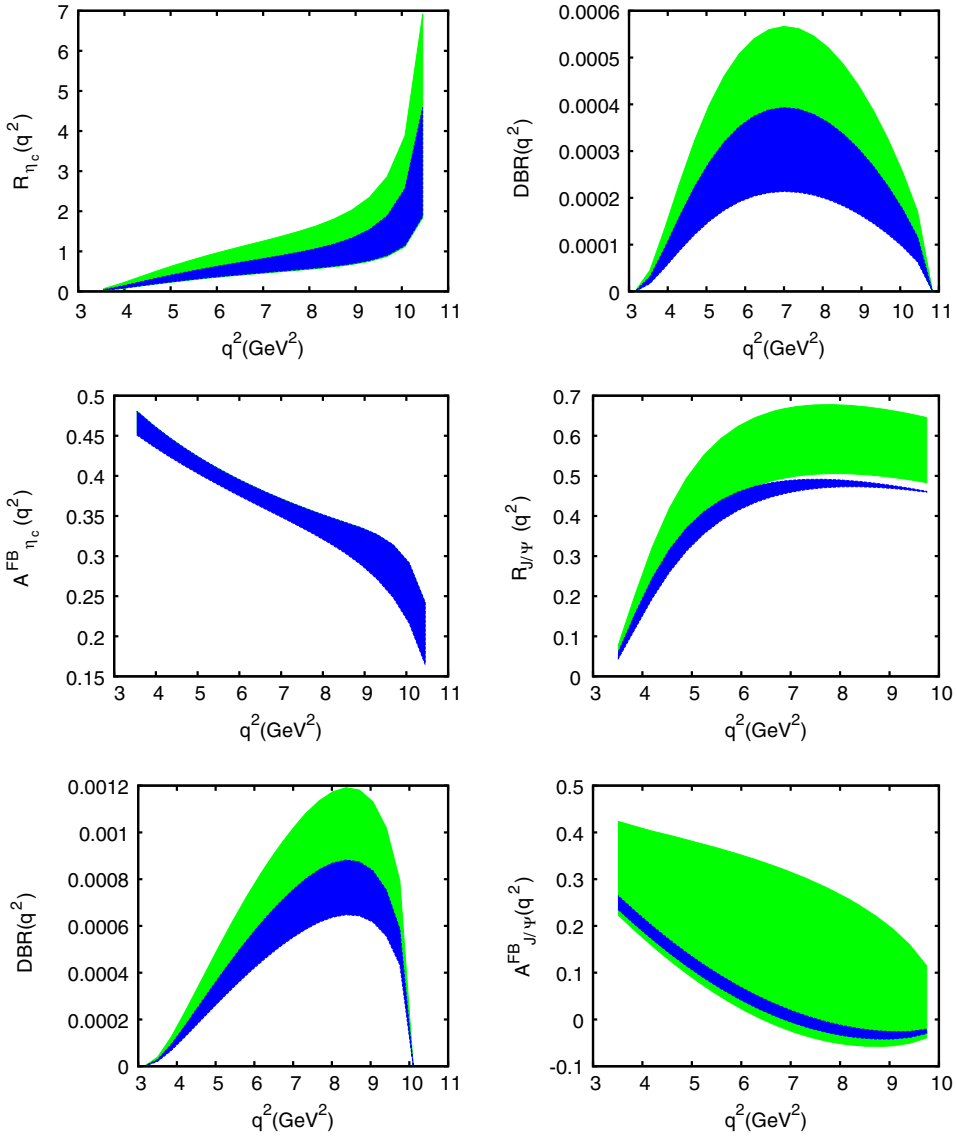

FIG. 3. Range in various q^2 dependent observables such as $\mathrm{DBR}(q^2)$, $R(q^2)$, and $A^{FB}(q^2)$ for the $B_c \to \eta_c \tau\nu$ (upper panel) and $B_c \to J/\Psi\tau\nu$ (lower panel) decays. The allowed range in each observable is shown in the light (green) band once the NP couplings (V_L, V_R) are varied within the allowed ranges shown in the left panel of Fig. 1. We show in the dark (blue) band the corresponding SM prediction.

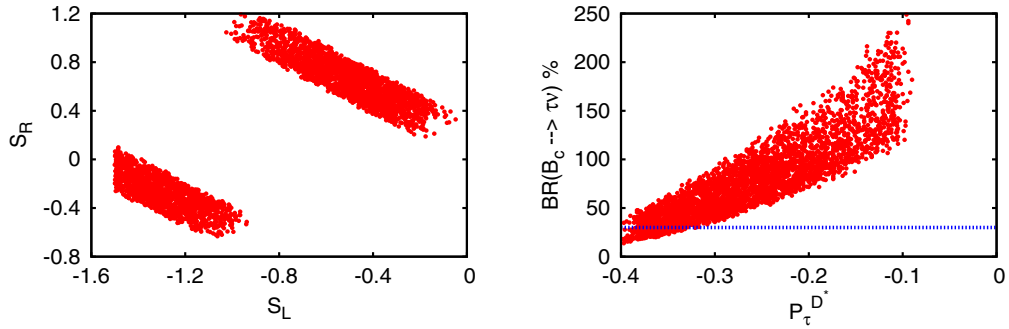

FIG. 4. Allowed ranges of S_L and S_R NP couplings are shown in the left panel once the 2σ constraint coming from the measured values of the ratio of branching ratios R_D and R_{D^*} is imposed. We show in the right panel the allowed ranges in $\mathcal{B}(B_c \to \tau\nu)$ and $P_\tau^{D^*}$ in the presence of these NP couplings. The blue constant line in the right panel corresponds to $\mathcal{B}(B_c \to \tau\nu) = 30\%$.

TABLE VI. Allowed ranges of various observables in the presence of S_L and S_R NP couplings.

Observables	Range	Observables	Range	Observables	Range
$\mathcal{B}(B_c \to \tau\nu) \times 10^2$	[13.84, 248.94]	R_{η_c}	[0.213, 0.706]	$P_\tau^{J/\Psi}$	$[-0.405, 0.117]$
$\mathcal{B}(B_c \to \eta_c\tau\nu) \times 10^3$	[1.05, 3.02]	$R_{J/\Psi}$	[0.299, 0.486]	P_τ^{D}	[0.301, 0.597]
$\mathcal{B}(B_c \to J/\Psi\tau\nu) \times 10^3$	[3.08, 5.71]	$P_\tau^{\eta_c}$	[0.053, 0.714]	$P_\tau^{D^*}$	$[-0.090, -0.398]$

$B_c \to \eta_c\tau\nu$ decay mode. It is expected as the NP dependency cancels in the ratio since the $B_c \to \eta_c\tau\nu$ decay mode depends on G_V couplings only. However, we see significant deviation of $A_{J/\Psi}^{FB}(q^2)$ from the SM prediction. It is mainly because of the presence of G_V as well as G_A couplings. It is also evident from Fig. 3 that although there is no zero crossing in the $A_{\eta_c}^{FB}(q^2)$ parameter for the $B_c \to \eta_c\tau\nu$ decay mode, there is a zero crossing in the $A_{J/\Psi}^{FB}(q^2)$ parameter at $q^2 \equiv 7.0\ \mathrm{GeV}^2$ in the SM for the $B_c \to J/\Psi\tau\nu$ decay mode. It should be noted that, in the presence of such NP, depending on the value of V_L and V_R, there may or may not be a zero crossing for the $B_c \to J/\Psi\tau\nu$ decay mode which can be quite different from the SM prediction.

2. Scenario II: Only S_L and S_R NP couplings

In this scenario, we vary only the new scalar interactions S_L and S_R while keeping all other NP couplings to zero. We restrict the S_L and S_R parameter space using the 2σ experimental constraint coming from measured values of R_D and R_{D^*}. The allowed range of S_L and S_R is shown in the left panel of Fig. 4. We also show in the right panel of Fig. 4 the allowed ranges of $\mathcal{B}(B_c \to \tau\nu)$ and $P_\tau^{D^*}$ in this scenario. We see significant deviation of all the observables from the SM expectation in this scenario. It is also worth mentioning that the tau polarization $P_\tau^{D^*}$ deviates significantly from the central value reported by BELLE. However, the uncertainty associated with the measured value of $P_\tau^{D^*}$ is rather large. Again, we notice that, in this scenario, the value of $\mathcal{B}(B_c \to \tau\nu)$ can exceed the total decay width of the B_c meson for some particular values of S_L and S_R. We note that only $\leq 5\%$ of the total decay width of the B_c meson can be explained by semitaunic decays. However, this constraint can be relaxed up to 30%. If we assume that $\mathcal{B}(B_c \to \tau\nu)$ cannot be greater than 5%, then although S_L and S_R type NP couplings can explain the anomalies in R_D and R_{D^*}, it, however, cannot accommodate $\mathcal{B}(B_c \to \tau\nu)$. It is evident from the right panel of Fig. 4 that even with a 30% constraint, a large part of the NP parameter space preferred by R_D and R_{D^*} can be excluded. The allowed

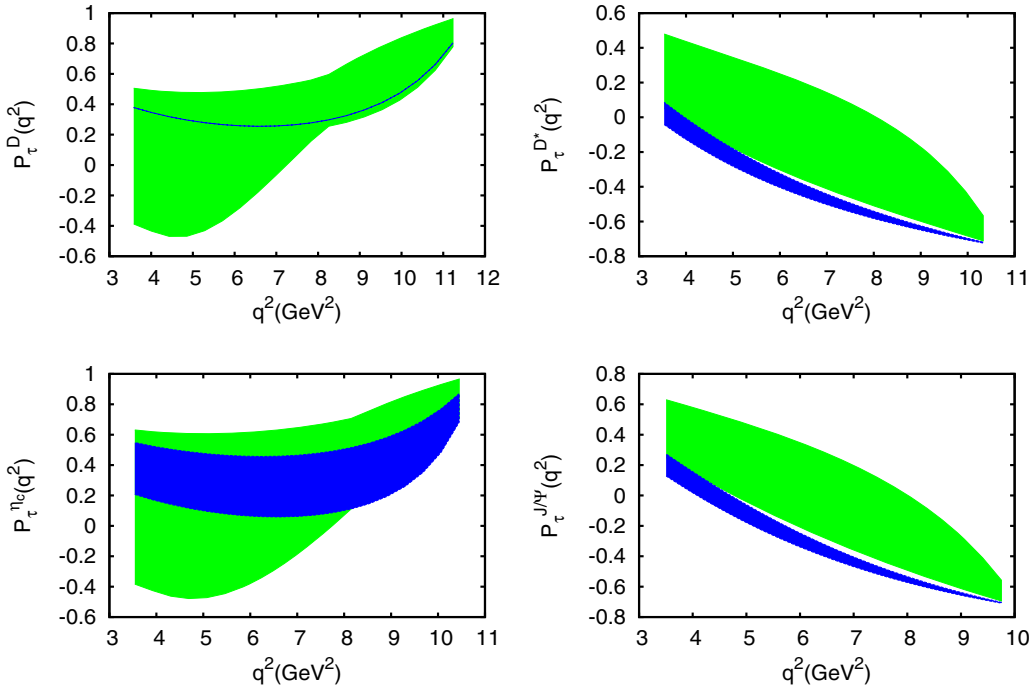

FIG. 5. Range in $P_\tau(q^2)$ for the $B \to (D, D^*)\tau\nu$ (upper panel) and $B_c \to (\eta_c, J/\Psi)\tau\nu$ (lower panel) decays. The allowed range in each observable is shown in the light (green) band once the NP couplings (S_L, S_R) are varied within the allowed ranges shown in the left panel of Fig. 4. We show in the dark (blue) band the corresponding SM prediction.

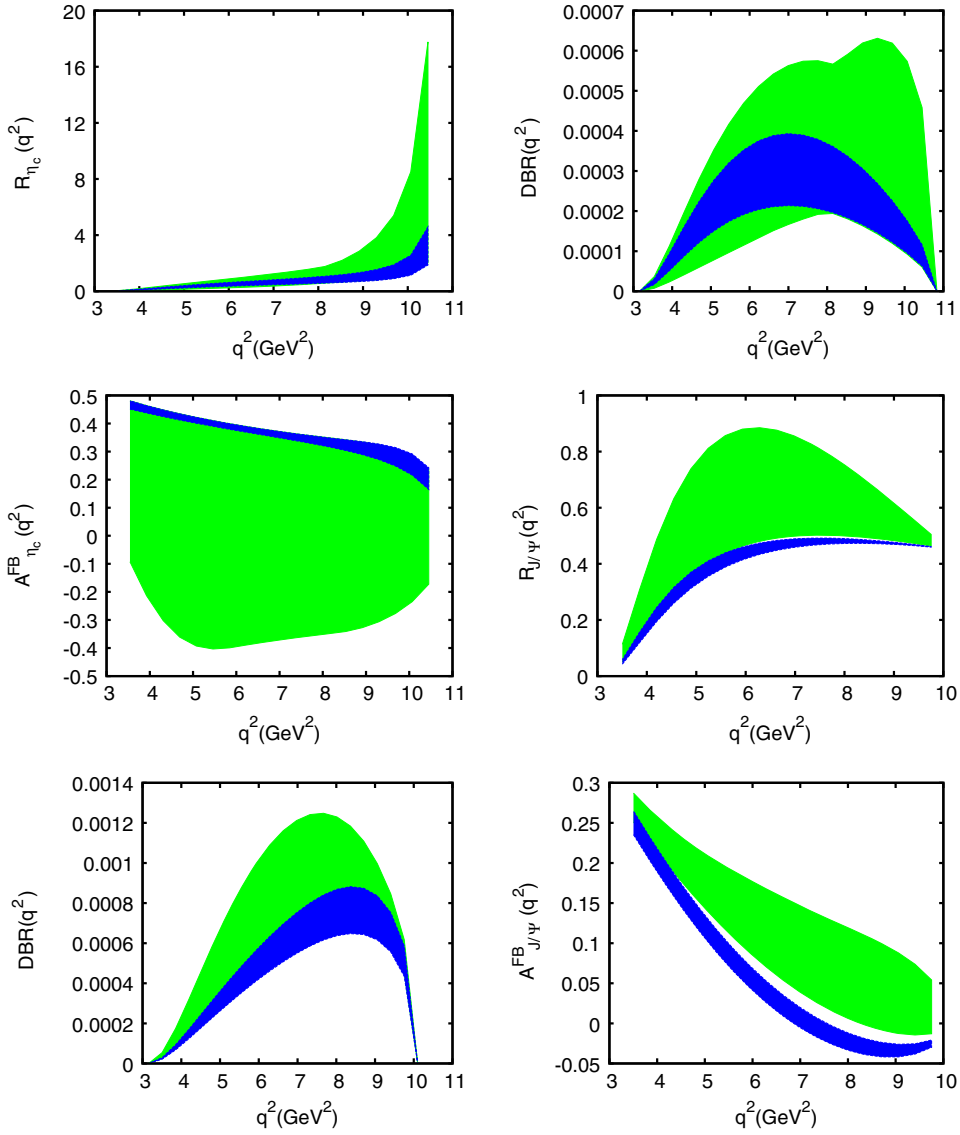

FIG. 6. Range in various q^2 dependent observables such as DBR(q^2), $R(q^2)$, and $A^{FB}(q^2)$ for the $B_c \to \eta_c \tau\nu$ (upper panel) and $B_c \to J/\Psi\tau\nu$ (lower panel) decays. The allowed range of each observable is shown in the light (green) band once the NP couplings (S_L, S_R) are varied within the allowed ranges shown in the left panel of Fig. 4. We show in the dark (blue) band the corresponding SM prediction.

ranges of each observable obtained in the presence of S_L and S_R NP couplings are tabulated in Table VI. It should be noted that, unlike scenario I, the deviation observed in this scenario is rather large.

We show in Fig. 5 the effect of new scalar couplings S_L and S_R on the τ polarization parameter $P_\tau(q^2)$ for the $B \to (D, D^*)\tau\nu$ and $B_c \to (\eta_c, J/\Psi)\tau\nu$ decays. We see significant deviation from the SM prediction. We note that although there is no zero crossing in P_τ^D and $P_\tau^{\eta_c}$ in the SM, there may or may not be zero crossing depending on the new scalar couplings S_L and S_R. It should be emphasized that the zero crossing in the τ polarization parameter for the $B \to D^*\tau\nu$ and $B_c \to J/\Psi\tau\nu$ decays may shift towards the higher values of q^2 once the NP couplings S_L and S_R are switched on.

We wish to see the effect of S_L and S_R NP couplings on various other q^2 dependent observables such as the ratio of the branching ratio $R(q^2)$, forward-backward asymmetry $A^{FB}(q^2)$, and the differential branching ratio DBR(q^2) for the $B_c \to (\eta_c, J/\Psi)\tau\nu$ decays. The effect of NP couplings on these observables is shown in Fig. 6. Significant deviation from the SM expectation is observed for all the observables in this scenario. We see that, in this scenario, all the observables are quite sensitive to the NP couplings for $B_c \to \eta_c\tau\nu$ and $B_c \to J/\Psi\tau\nu$ decay modes. The deviation from the SM prediction observed

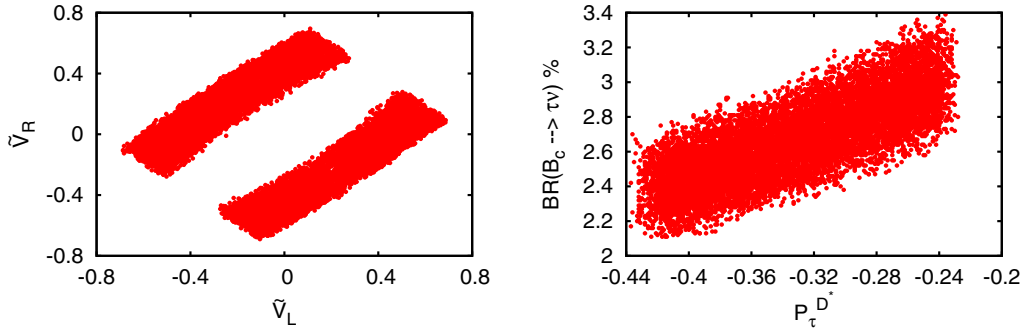

FIG. 7. Allowed ranges of $\tilde{V}_L$ and $\tilde{V}_R$ NP couplings are shown in the left panel once a 2σ constraint coming from the measured values of the ratio of branching ratios R_D and R_{D^*} is imposed. We show in the right panel the allowed ranges in $\mathcal{B}(B_c \to \tau\nu)$ and $P_\tau^{D^*}$ in the presence of these NP couplings.

in the case of the $B_c \to \eta_c\tau\nu$ decay mode is quite different from that of the $B_c \to J/\Psi\tau\nu$ decay mode. It is expected as the former decay mode depends on the NP couplings through G_S, whereas, the latter depends on the NP couplings through G_P. Again, the peak of the q^2 distribution of differential branching ratio for the $B_c \to \eta_c\tau\nu$ decays may shift towards a higher q^2 region once such NP couplings are present. However, for the $B_c \to J/\Psi\tau\nu$ decays, the peak may shift towards a lower q^2 region in the presence of such NP. We also observe that, although in the SM there is no zero crossing in the forward-backward asymmetry parameter for the $B_c \to \eta_c\tau\nu$ decays, depending on the value of new scalar couplings S_L and S_R, we might observe a zero crossing for this decay mode. Again, for the $B_c \to J/\Psi\tau\nu$ decay mode, the zero crossing point may shift towards the higher q^2 region in the presence of such NP couplings. It is worth mentioning that the $A^{FB}(q^2)$ parameter in the case of $B_c \to \eta_c\tau\nu$ decays is more sensitive to such NP couplings than that of $B_c \to J/\Psi\tau\nu$ decays.

3. Scenario III: Only $\tilde{V}_L$ and $\tilde{V}_R$ NP couplings

In this scenario, we wish to see the effect of right-handed neutrino couplings $\tilde{V}_L$ and $\tilde{V}_R$ on various observables. To realize this we vary only $\tilde{V}_L$ and $\tilde{V}_R$ and fix all other NP couplings to zero. The allowed ranges of $\tilde{V}_L$ and $\tilde{V}_R$ obtained by using the 2σ constraint coming from the measured values of the ratio of branching ratios R_D and R_{D^*} are shown in the left panel of Fig. 7. We see a less constrained NP parameter space as the decay rate depends on these couplings quadratically. The effect of $\tilde{V}_L$ and $\tilde{V}_R$ NP couplings on various observables are reported in Table VII. We also show, in particular, the effect of $\tilde{V}_L$ and $\tilde{V}_R$ on the branching ratio of $B_c \to \tau\nu$ and the on tau polarization fraction $P_\tau^{D^*}$ in the right panel of Fig. 7. The $B_c \to \tau\nu$ branching ratio obtained in this scenario is compatible with the total decay width of the B_c meson. We also note that the central value of the τ polarization fraction $P_{D^*}^{\tau}$ reported by BELLE lies outside the allowed range obtained in this scenario. It, however, should be mentioned that the error associated with the BELLE reported value on $P_\tau^{D^*}$ is quite large. More precise data on $P_\tau^{D^*}$ in the future will help in constraining the NP parameter space even more. Deviation from the SM expectation observed is quite large in this scenario.

In Fig. 8, we show the effect of $\tilde{V}_L$ and $\tilde{V}_R$ NP couplings on the τ polarization fraction for the $B \to (D, D^*)\tau\nu$ and $B_c \to (\eta_c, J/\Psi)\tau\nu$ decay modes. We see a significant deviation of this parameter from the SM expectation. Although, the differential decay branching ratio for the $B \to D\tau\nu$ and $B_c \to \eta_c\tau\nu$ decays depends on $\tilde{G}_V$ only, there is no cancellation of the NP effects because of the contribution coming from the SM left-handed currents. We do not observe any zero crossing for the tau polarization parameter P_τ^D and $P_\tau^{\eta_c}$ with and without NP. However, depending on the values of the $\tilde{V}_L$ and $\tilde{V}_R$ NP couplings, it may be quite different from the SM expectation.

The allowed ranges of various other q^2 dependent observables such as the ratio of the branching ratio $R(q^2)$, the forward-backward asymmetry $A^{FB}(q^2)$, and the differential branching ratio $\mathrm{DBR}(q^2)$ for the $B_c \to (\eta_c, J/\Psi)\tau\nu$ decays are shown in Fig. 9. The SM prediction is shown in a dark (blue) band whereas the effect of NP

TABLE VII. Allowed ranges of various observables in the presence of $\tilde{V}_L$ and $\tilde{V}_R$ NP couplings.

Observables	Range	Observables	Range	Observables	Range
$\mathcal{B}(B_c \to \tau\nu) \times 10^2$	[2.11, 3.39]	R_{η_c}	[0.238, 0.690]	$P_\tau^{J/\Psi}$	$[-0.189, -0.437]$
$\mathcal{B}(B_c \to \eta_c\tau\nu) \times 10^3$	[1.11, 3.07]	$R_{J/\Psi}$	[0.296, 0.416]	P_τ^D	[0.070, 0.338]
$\mathcal{B}(B_c \to J/\Psi\tau\nu) \times 10^3$	[3.08, 5.19]	$P_\tau^{\eta_c}$	[0.042, 0.523]	$P_\tau^{D^*}$	$[-0.228, -0.437]$

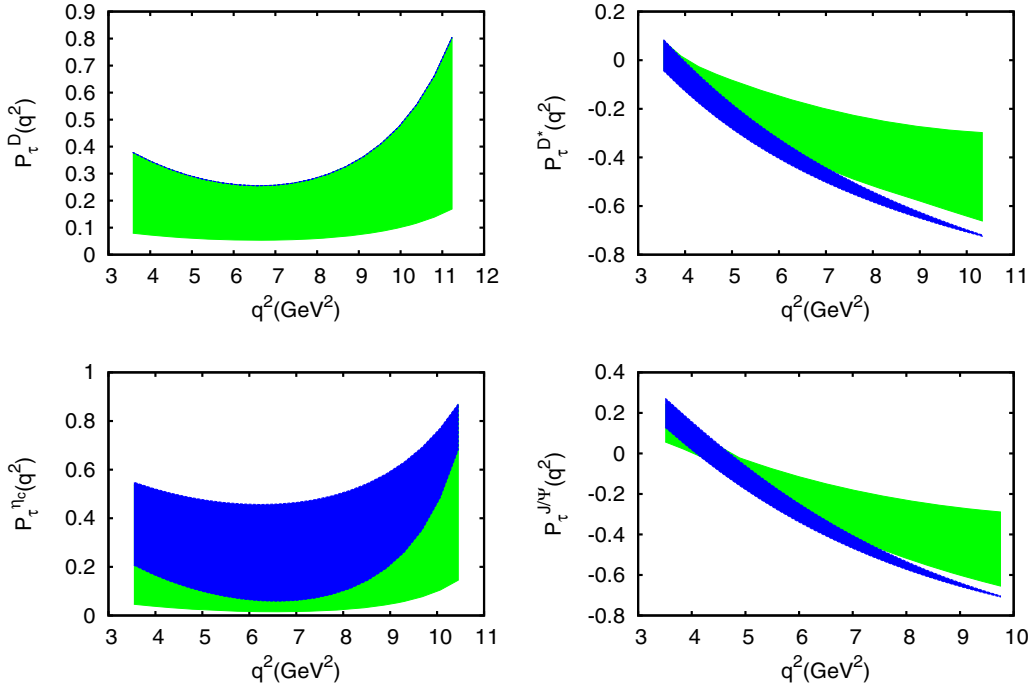

FIG. 8. Range in $P_\tau(q^2)$ for the $B \to (D, D^*)\tau\nu$ (upper panel) and $B_c \to (\eta_c, J/\Psi)\tau\nu$ (lower panel) decays. The allowed range in each observable is shown in the light (green) band once the NP couplings $(\tilde{V}_L, \tilde{V}_R)$ are varied within the allowed ranges shown in the left panel of Fig. 7. We show in the dark (blue) band the corresponding SM prediction.

couplings is shown in a light (green) band. The q^2 distribution looks quite similar to what we obtain in scenario I of Sec. III B 1. Although we see a significant deviation of all the observables in this scenario, the forward-backward asymmetry parameter $A_{\eta_c}^{FB}(q^2)$ for the $B_c \to \eta_c\tau\nu$ decay mode does not seem to vary with the $\tilde{V}_L$ and $\tilde{V}_R$ NP couplings. This is obvious because the $B_c \to \eta_c\tau\nu$ differential branching ratio depends only on $\tilde{G}_V$ and hence the NP effect gets canceled in the ratio. On the other hand, the $B_c \to J/\Psi\tau\nu$ decay differential branching ratio depends not only on $\tilde{G}_V$ but also on $\tilde{G}_A$ and no such cancellation of the NP effects in the forward-backward asymmetry parameter occurs for this decay mode. Hence we observe a significant deviation of $A_{J/\Psi}^{FB}$ from the SM expectation. Again, depending on these NP couplings, there may or may not be a zero crossing in $A_{J/\Psi}^{FB}(q^2)$ parameter which can be quite different from the SM prediction.

4. Scenario IV: Only $\tilde{S}_L$ and $\tilde{S}_R$ NP couplings

To see the effect of new $\tilde{S}_L$ and $\tilde{S}_R$ couplings, associated with the right-handed neutrino, on various observables we vary $\tilde{S}_L$ and $\tilde{S}_R$ while keeping all other NP couplings to zero. We impose the 2σ constraint coming from the measured values of the ratio of branching ratios R_D and R_{D^*} and the resulting allowed ranges of $\tilde{S}_L$ and $\tilde{S}_R$ NP couplings are shown in the left panel of Fig. 10. The decay rate depends on $\tilde{S}_L$ and $\tilde{S}_R$ NP couplings quadratically and we obtain a less constrained NP parameter space. We also show in the right panel of Fig. 10 the allowed ranges of $\mathcal{B}(B_c \to \tau\nu)$ and the tau polarization fraction $P_\tau^{D^*}$. We note that the central value of $P_\tau^{D^*}$ reported by BELLE lies outside the allowed range obtained in this scenario. Again, the branching ratio of $B_c \to \tau\nu$ decays obtained in this scenario is rather large, more than 45%. However, from the total decay width of the B_c meson one can infer that the branching ratio of $B_c \to \tau\nu$ decays should not be more than 5%. Even if we relax the constraint up to 30%, the $\tilde{S}_L$ and $\tilde{S}_R$ NP couplings are ruled out although it can explain the anomalies that persisted in the ratio of branching ratios R_D and R_{D^*}. The allowed ranges of each observable obtained in this scenario are reported in Table VIII. All the observables are very sensitive to the new $\tilde{S}_L$ and $\tilde{S}_R$ NP couplings.

The effect of these NP couplings on the τ polarization parameter $P_\tau(q^2)$ for the $B \to (D, D^*)\tau\nu$ and $B_c \to (\eta_c, J/\Psi)\tau\nu$ decay modes are shown in Fig. 11. Similar to scenario II, we see significant deviation from the SM prediction. The deviation observed in the case of the $B \to D\tau\nu$ decays is quite similar to that of $B_c \to \eta_c\tau\nu$ decays since the differential branching ratio for these decay modes depend on these NP couplings through $\tilde{G}_S^2$. A similar conclusion can be drawn for the $B \to D^*\tau\nu$ and $B_c \to J/\Psi\tau\nu$ decays as well since the differential branching ratio for these decay modes depend on NP couplings through $\tilde{G}_P^2$. Again, it should be noted that although there is no zero

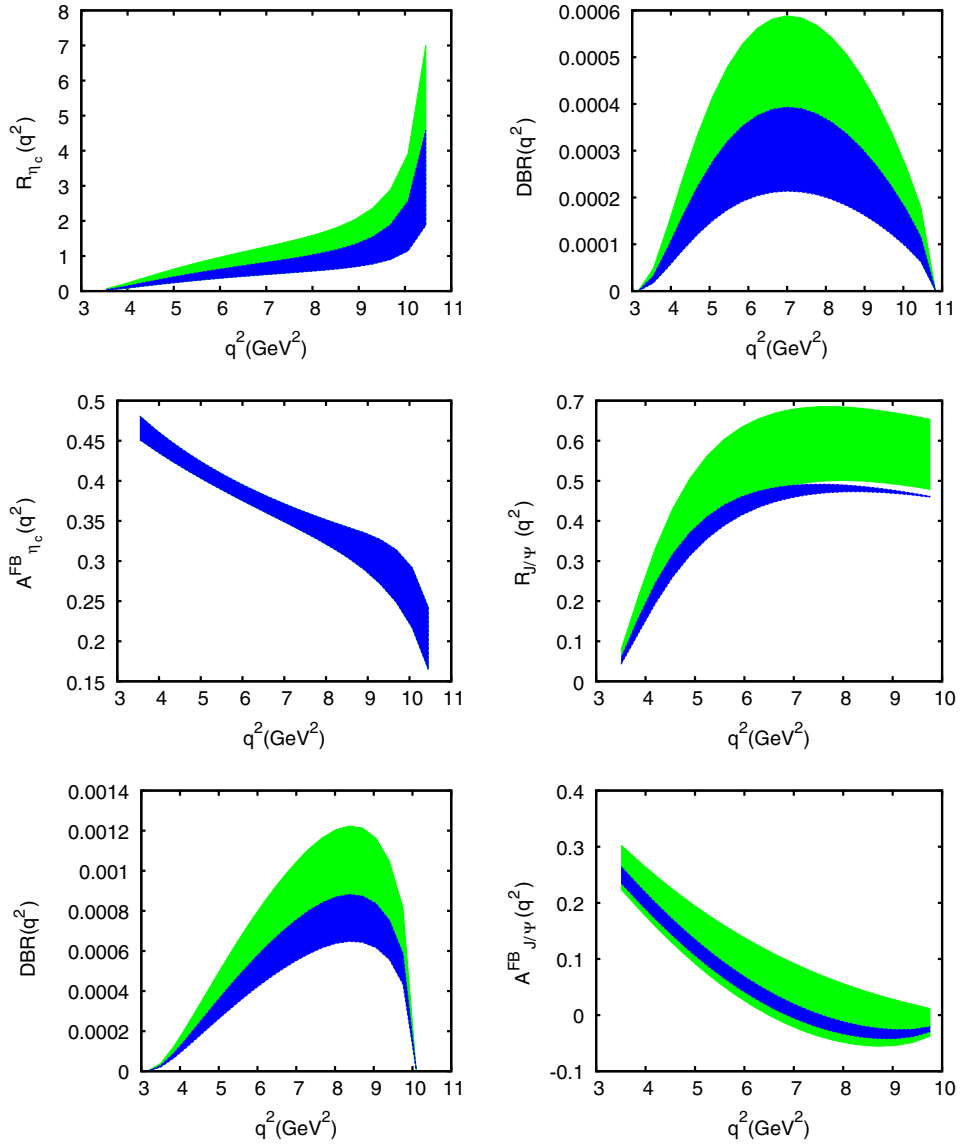

FIG. 9. Range in various q^2 dependent observables such as $\mathrm{DBR}(q^2)$, $R(q^2)$, and $A^{FB}(q^2)$ for the $B_c \to \eta_c\tau\nu$ (upper panel) and $B_c \to J/\Psi\tau\nu$ (lower panel) decays. The allowed range of each observable is shown in the light (green) band once the NP couplings $(\tilde{V}_L, \tilde{V}_R)$ are varied within the allowed ranges shown in the left panel of Fig. 7. We show in the dark (blue) band the corresponding SM prediction.

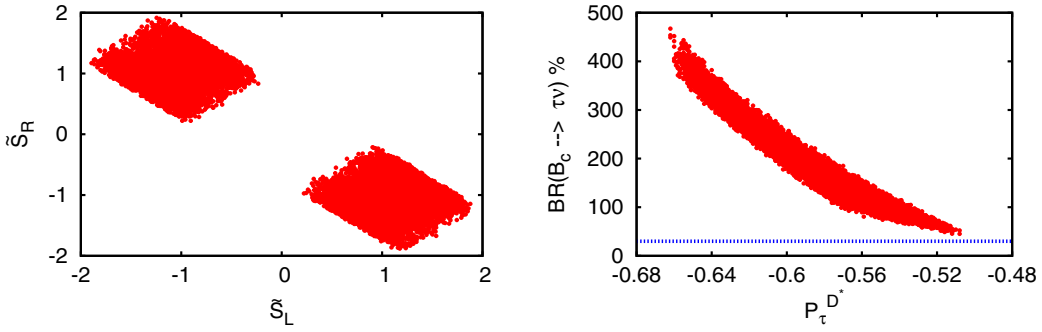

FIG. 10. Allowed ranges of $\tilde{S}_L$ and $\tilde{S}_R$ NP couplings are shown in the left panel once the 2σ constraint coming from the measured values of the ratio of branching ratios R_D and R_{D^*} is imposed. We show in the right panel the allowed ranges in $\mathcal{B}(B_c \to \tau\nu)$ and $P_\tau^{D^*}$ in the presence of these NP couplings. The blue constant line in the right panel corresponds to $\mathcal{B}(B_c \to \tau\nu) = 30\%$.

TABLE VIII. Allowed ranges of various observables in the presence of $\tilde{S}_L$ and $\tilde{S}_R$ NP couplings.

Observables	Range	Observables	Range	Observables	Range
$\mathcal{B}(B_c \to \tau\nu) \times 10^2$	[45.14, 467.22]	R_{η_c}	[0.238, 0.696]	$P_\tau^{J/\Psi}$	$[-0.478, -0.660]$
$\mathcal{B}(B_c \to \eta_c\tau\nu) \times 10^3$	[1.10, 3.15]	$R_{J/\Psi}$	[0.299, 0.490]	P_τ^{D}	$[-0.190, 0.338]$
$\mathcal{B}(B_c \to J/\Psi\tau\nu) \times 10^3$	[3.08, 5.79]	$P_\tau^{\eta_c}$	$[-0.210, 0.523]$	$P_\tau^{D^*}$	$[-0.508, -0.662]$

crossing in the τ polarization parameter P_τ^D and $P_\tau^{\eta_c}$ in the SM, there may or may not be a zero crossing depending on the value of NP couplings $\tilde{S}_L$ and $\tilde{S}_R$. Similarly, although there is zero crossing in the τ polarization parameter $P_\tau^{D^*}$ and $P_\tau^{J/\Psi}$ in the SM, it may or may not be present depending on the NP couplings $\tilde{S}_L$ and $\tilde{S}_R$. Depending on these NP couplings, the tau polarization fraction can be quite different from the SM expectation.

The allowed ranges of various q^2 dependent observables such as $R(q^2)$, $A^{FB}(q^2)$, and $\mathrm{DBR}(q^2)$ for the $B_c \to \eta_c\tau\nu$ and $B_c \to J/\Psi\tau\nu$ decay modes are shown in Fig. 12. We see that all the observables deviate significantly from the SM expectation. Variation in $B_c \to \eta_c\tau\nu$ and $B_c \to J/\Psi\tau\nu$ decays, however, are quite different. This is what we expect because $B_c \to \eta_c\tau\nu$ decay branching ratio depends on these NP couplings through the $\tilde{G}_S$ term, whereas the $B_c \to J/\Psi\tau\nu$ decay branching ratio depends on these NP couplings through the $\tilde{G}_P$ term. Although the effects of $\tilde{S}_L$ and $\tilde{S}_R$ NP couplings are quite similar to the S_L and S_R NP couplings of Sec. III B 2, there are some differences. Unlike scenario II, we do not observe any zero crossing in the q^2 distribution of the forward-backward asymmetry parameter $A_{\eta_c}^{FB}$ in the presence of such NP.

IV. CONCLUSION

Deviations from the SM prediction have been observed not only in decays mediated via the $b \to c$ charged current process but also in decays mediated via the $b \to s$ neutral current process. In particular, the deviation of the measured ratios R_D and R_{D^*} from the SM prediction is more pronounced and it currently stands at the 3.9σ level. Similarly, there are significant deviations from the SM prediction in $b \to sl^+l^-$ decays as well. The measured ratio R_K deviates from the SM prediction by 2.6σ. Again, various other interesting tensions between the experimental results and SM prediction have been observed in rare $B \to K^*\mu^+\mu^-$ and $B \to \phi\mu^+\mu^-$ decays. Very recently the LHCb has measured R_{K^*}, the ratio of the branching ratios

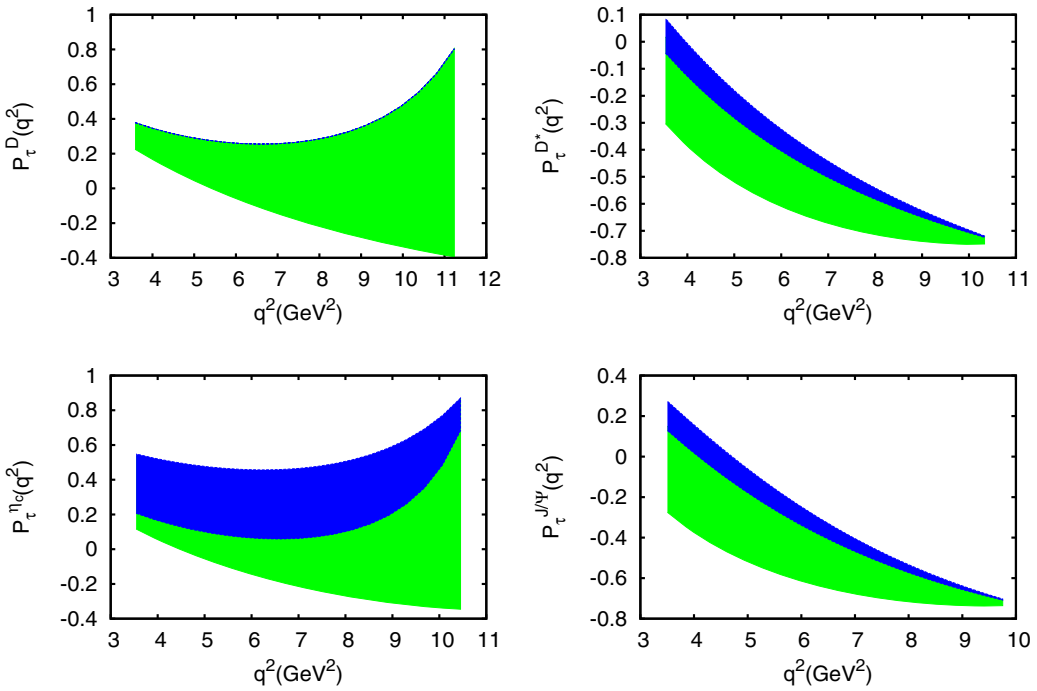

FIG. 11. Range in $P_\tau(q^2)$ for the $B \to (D, D^*)\tau\nu$ (upper panel) and $B_c \to (\eta_c, J/\Psi)\tau\nu$ (lower panel) decays. The allowed range in each observable is shown in the light (green) band once the NP couplings $(\tilde{S}_L, \tilde{S}_R)$ are varied within the allowed ranges shown in the left panel of Fig. 10. We show in the dark (blue) band the corresponding SM prediction.

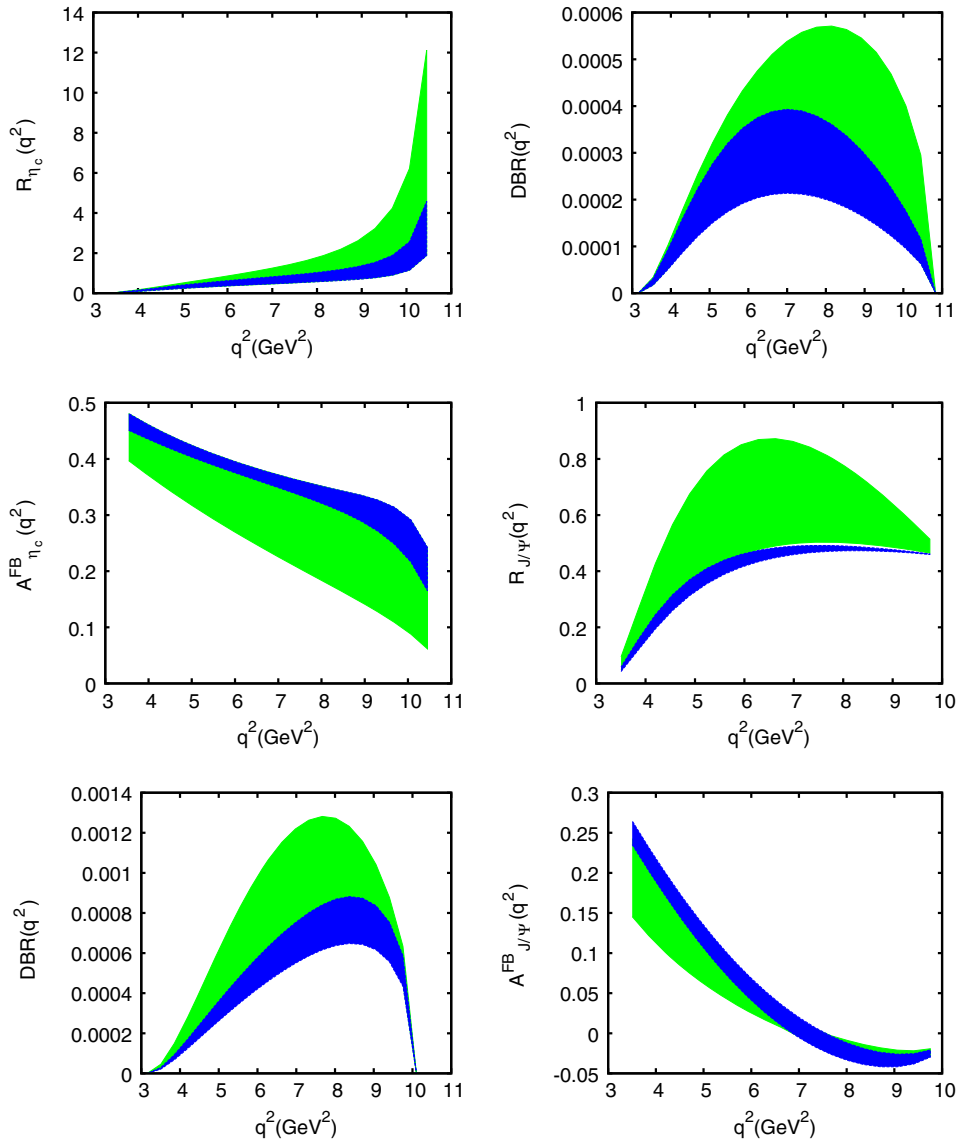

FIG. 12. Range in various q^2 dependent observables such as DBR(q^2), $R(q^2)$, and $A^{FB}(q^2)$ for the $B_c \to \eta_c\tau\nu$ (upper panel) and $B_c \to J/\Psi\tau\nu$ (lower panel) decays. The allowed range for each observable is shown in the light (green) band once the NP couplings $(\tilde{S}_L, \tilde{S}_R)$ are varied within the allowed ranges shown in the left panel of Fig. 10. We show in the dark (blue) band the corresponding SM prediction.

of $B \to K^*\mu\mu$ to that of $B \to K^*ee$. Approximately 2.5σ deviations from the SM prediction have been observed for R_{K^*} in the dilepoton invariant mass $q^2 = [0.045\text{–}1.1]$ GeV^2 and $[1.1\text{–}6]$ GeV^2 [99]. If it persists and is confirmed by future experiments, these could provide the necessary information to unravel the flavor structure of beyond the SM physics. The study of $B_c \to \eta_c\tau\nu$ and $B_c \to J/\Psi\tau\nu$ decays is interesting because, similar to $B \to (D, D^*)\tau\nu$ decays, these decays are also mediated via $b \to c$ charged current interactions. Thus, if NP is present in the $B \to (D, D^*)\tau\nu$ decays, then it would show up in these decay modes as well. A detailed study of these decay modes theoretically as well as experimentally is necessary in order to explore physics beyond the SM. Although, a SM prediction of various observables related to these decay modes has been reported by various authors, the NP contribution has not been studied in detail. To see the effect of NP on various observables, we consider the effective theory formalism in the presence of NP for the $b \to cl\nu$ process. We assume that NP is present only for the third generation leptons. We study four different NP scenarios. We summarize our results below.

We first report the central values and the 1σ ranges of all the observables within the SM. The branching ratios of $B_c \to \eta_c\tau\nu$ and $B_c \to J/\Psi\tau\nu$ decays are at the order of 10^{-3}. Again, we find the branching ratio of $B_c \to \tau\nu$ to be of the order of 2%. The values of the ratio of branching ratios R_{η_c} and $R_{J/\Psi}$ are quite similar to the values reported

in Ref. [86]. We also give the first prediction of the tau polarization fraction $P_\tau^{\eta_c}$ and $P_\tau^{J/\Psi}$ for the $B_c \to \eta_c \tau\nu$ and $B_c \to J/\Psi\tau\nu$ decay modes.

We include vector and scalar type NP interactions that involve both right-handed as well as left-handed neutrinos in our analysis and explore four different NP scenarios. In the first scenario, we consider only vector type NP interactions that involve left-handed neutrinos. We vary V_L and V_R while keeping all other NP couplings to zero. Deviation from the SM expectation is observed for all the observables. The central value of $P_\tau^{D^*}$ reported by BELLE lies outside the allowed range of $P_\tau^{D^*}$ obtained in this scenario. However, the uncertainty associated with the measured value of $P_\tau^{D^*}$ is rather large. More precise data in the future on $P_\tau^{D^*}$ will definitely help in constraining the NP parameter space even more. The allowed range of $\mathcal{B}(B_c \to \tau\nu)$ is consistent with the total decay width of the B_c meson. We see no deviation from the SM prediction of the tau polarization fraction P_τ^D and $P_\tau^{\eta_c}$ as the NP effects coming from V_L and V_R couplings cancel in the ratios. We also see the effect of these NP couplings on various q^2 dependent observables. Significant deviation from the SM expectation is observed once the NP couplings are included. There is, however, no deviation from the SM prediction of the forward-backward asymmetry parameter $A_{\eta_c}^{FB}$. Similarly, we do not observe any deviation from the SM prediction of the τ polarization parameter $P_\tau^M(q^2)$ for all the decay modes.

In the second scenario, we consider that the NP effect is due to the scalar type interactions that involve left-handed neutrinos only, i.e, $S_{L,R} \neq 0$, whereas all other NP couplings are zero. Significant deviation from the SM expectation is observed for all the observables. It is also worth mentioning that the tau polarization $P_\tau^{D^*}$ deviates significantly from the central value reported by BELLE. Again, we notice that, in this scenario, for some particular values of S_L and S_R, the value of $\mathcal{B}(B_c \to \tau\nu)$ exceeds the total decay width of the B_c meson. However, only less than 5% of the total decay width of the B_c meson can be explained by the semi(taunic) mode. Even if we relaxed the constraint up to 30%, a substantial part of NP parameter space can be excluded. Hence, the B_c total decay width put a severe constraint on S_L and S_R type NP couplings. We also see the effect of NP couplings on various q^2 dependent observables. The deviation observed in this scenario is more pronounced than the deviation observed in scenario I.

In the third scenario, we set $\tilde{V}_{L,R} \neq 0$ while keeping all other NP couplings to zero. Similar to scenario I, we see a significant deviation of all the observables from the SM prediction. We want to mention that, the branching ratio of $B_c \to \tau\nu$ obtained in this scenario is consistent with the experimentally measured total decay width of the B_c meson. Again, although the central value of $P_\tau^{D^*}$ reported by BELLE lies outside the allowed range obtained, the 1σ range of the experimental value does overlap with the allowed range. More precise data on the $P_\tau^{D^*}$ observable is needed to constrain the NP parameter even further. The deviation in various q^2 dependent observables observed in this scenario is similar to the ones that we observed in scenario I. The forward-backward asymmetry parameter $A_{\eta_c}^{FB}$ does not vary at all as the NP dependency cancels in the ratio. However, a significant deviation from the SM prediction is observed for the τ polarization parameter $P_\tau^M(q^2)$ in this scenario.

In the fourth scenario we consider only $\tilde{S}_L$ and $\tilde{S}_R$ type NP couplings. Again, as expected, the deviations from the SM prediction in this scenario are quite large. We notice that the branching ratio of $B_c \to \tau\nu$ decays obtained in this scenario is rather large, more than 45%. However, from the total decay width of the B_c meson one can infer that the branching ratio of $B_c \to \tau\nu$ decays should not be more than 5%. Even if the constraint is relaxed up to 30%, the $\tilde{S}_L$ and $\tilde{S}_R$ NP couplings are ruled out although it can explain the anomalies that persisted in the ratio of branching ratios R_D and R_{D^*}. It is worth mentioning that all the observables are very sensitive to the new $\tilde{S}_L$ and $\tilde{S}_R$ NP couplings, similar to scenario II. All the q^2 dependent observables are also very sensitive to the new $\tilde{S}_L$ and $\tilde{S}_R$ NP couplings.

In conclusion, we observe that the B_c lifetime put a severe constraint on $S_{L,R}$ and $\tilde{S}_{L,R}$ type NP couplings. More precise calculations of the B_c lifetime and measurements of the branching fractions of its various decay channels in the future should help constrain the NP parameter space even further. Again, the observable $P_\tau^{D^*}$ has the potential to distinguish between various NP scenarios once more precise data is available. At present, however, the experimental uncertainty associated with the tau polarization fraction $P_\tau^{D^*}$ is rather large. More precise data in the future will definitely help in identifying the nature of NP. The measurement of all the observables for the $B_c \to \eta_c\tau\nu$ and $B_c \to J/\Psi\tau\nu$ decay modes will be crucial to explore the nature of NP patterns. It is worth mentioning that improved theoretical estimates of various B_c meson form factors would be crucial to look for possible new physics effects in $B_c \to \eta_c\tau\nu$ and $B_c \to J/\Psi\tau\nu$ decays. In this paper, we have used the form factors and the associated theoretical uncertainties reported in Ref. [86] at face value. Our conclusion may change once more precise estimates on these form factors are available. Again, more data samples from LHCb and BELLE II in the future will be needed to enhance the significance of R_D and R_{D^*} measurements and to disentangle genuine new physics effects from various statistical and systematic uncertainties.

[1] J. P. Lees *et al.* (*BABAR* Collaboration), Evidence for an Excess of $\bar{B} \to D^{(*)}\tau^-\bar{\nu}_\tau$ Decays, Phys. Rev. Lett. **109**, 101802 (2012).

[2] J. P. Lees *et al.* (*BABAR* Collaboration), Measurement of an excess of $\bar{B} \to D^{(*)}\tau^-\bar{\nu}_\tau$ decays and implications for charged Higgs bosons, Phys. Rev. D **88**, 072012 (2013).

[3] M. Huschle *et al.* (Belle Collaboration), Measurement of the branching ratio of $\bar{B} \to D^{(*)}\tau^-\bar{\nu}_\tau$ relative to $\bar{B} \to D^{(*)}\ell^-\bar{\nu}_\ell$ decays with hadronic tagging at Belle, Phys. Rev. D **92**, 072014 (2015).

[4] Y. Sato *et al.* (Belle Collaboration), Measurement of the branching ratio of $\bar{B}^0 \to D^{*+}\tau^-\bar{\nu}_\tau$ relative to $\bar{B}^0 \to D^{*+}\ell^-\bar{\nu}_\ell$ decays with a semileptonic tagging method, Phys. Rev. D **94**, 072007 (2016).

[5] A. Abdesselam *et al.*, Measurement of the τ lepton polarization in the decay $\bar{B} \to D^*\tau^-\bar{\nu}_\tau$, arXiv:1608.06391.

[6] R. Aaij *et al.* (LHCb Collaboration), Measurement of the Ratio of Branching Fractions $\mathcal{B}(\bar{B}^0 \to D^{*+}\tau^-\bar{\nu}_\tau)/\mathcal{B}(\bar{B}^0 \to D^{*+}\mu^-\bar{\nu}_\mu)$, Phys. Rev. Lett. **115**, 111803 (2015); Publisher's Note: Measurement of the Ratio of Branching Fractions, $\mathcal{B}(\bar{B}^0 \to D^{*+}\tau^-\bar{\nu}_\tau)/\mathcal{B}(\bar{B}^0 \to D^{*+}\mu^-\bar{\nu}_\mu)$, Phys. Rev. Lett. **115**, 159901(E) (2015).

[7] J. A. Bailey *et al.* (MILC Collaboration), $B \to D\ell\nu$ form factors at nonzero recoil and $|V_{cb}|$ from 2 + 1-flavor lattice QCD, Phys. Rev. D **92**, 034506 (2015).

[8] H. Na, C. M. Bouchard, G. P. Lepage, C. Monahan, and J. Shigemitsu (HPQCD Collaboration), $B \to Dl\nu$ form factors at nonzero recoil and extraction of $|V_{cb}|$, Phys. Rev. D **92**, 054510 (2015); Erratum: $B \to Dl\nu$ form factors at nonzero recoil and extraction of $|V_{cb}|$, Phys. Rev. D **93**, 119906 (2016).

[9] D. Bigi and P. Gambino, Revisiting $B \to D\ell\nu$, Phys. Rev. D **94**, 094008 (2016).

[10] S. Aoki *et al.*, Review of lattice results concerning low-energy particle physics, Eur. Phys. J. C **77**, 112 (2017).

[11] S. Fajfer, J. F. Kamenik, and I. Nisandzic, On the $B \to D^*\tau\bar{\nu}_\tau$ sensitivity to new physics, Phys. Rev. D **85**, 094025 (2012).

[12] Y. Amhis *et al.*, Averages of b-hadron, c-hadron, and τ-lepton properties as of summer 2016, arXiv:1612.07233.

[13] S. Fajfer, J. F. Kamenik, I. Nisandzic, and J. Zupan, Implications of Lepton Flavor Universality Violations in B Decays, Phys. Rev. Lett. **109**, 161801 (2012).

[14] W. S. Hou, Enhanced charged Higgs boson effects in $B^- \to \tau\bar{\nu}, \mu\bar{\nu}$, and $b \to \tau\bar{\nu} + X$, Phys. Rev. D **48**, 2342 (1993).

[15] A. G. Akeroyd and S. Recksiegel, "The Effect of $H^\pm$ on $B^\pm \to \tau^\pm\nu_\tau$ and $B^\pm \to \mu^\pm\nu_\mu$, J. Phys. G **29**, 2311 (2003).

[16] M. Tanaka, Charged Higgs effects on exclusive semi-tauonic B decays, Z. Phys. C **67**, 321 (1995).

[17] U. Nierste, S. Trine, and S. Westhoff, Charged-Higgs effects in a new $B \to D\tau\nu$ differential decay distribution, Phys. Rev. D **78**, 015006 (2008).

[18] T. Miki, T. Miura, and M. Tanaka, Effects of charged Higgs boson and QCD corrections in $\bar{B} \to D\tau\bar{\nu}_\tau$, arXiv:hep-ph/0210051.

[19] A. Wahab El Kaffas, P. Osland, and O. M. Ogreid, Constraining the two-Higgs-doublet-model parameter space, Phys. Rev. D **76**, 095001 (2007).

[20] O. Deschamps, S. Descotes-Genon, S. Monteil, V. Niess, S. T'Jampens, and V. Tisserand, Two Higgs doublet model of type II facing flavor physics data, Phys. Rev. D **82**, 073012 (2010).

[21] G. Blankenburg and G. Isidori, $B \to \tau\nu$ in two-Higgs doublet models with MFV, Eur. Phys. J. Plus **127**, 85 (2012).

[22] G. D'Ambrosio, G. F. Giudice, G. Isidori, and A. Strumia, Minimal flavor violation: An Effective field theory approach, Nucl. Phys. **B645**, 155 (2002).

[23] A. J. Buras, M. V. Carlucci, S. Gori, and G. Isidori, Higgs-mediated FCNCs: Natural Flavour Conservation vs. Minimal Flavour Violation, J. High Energy Phys. 10 (2010) 009.

[24] A. Pich and P. Tuzon, Yukawa alignment in the two-Higgs-doublet model, Phys. Rev. D **80**, 091702 (2009).

[25] M. Jung, A. Pich, and P. Tuzon, Charged-Higgs phenomenology in the aligned two-Higgs-doublet model, J. High Energy Phys. 11 (2010) 003.

[26] A. Crivellin, C. Greub, and A. Kokulu, Explaining $B \to D\tau\nu$, $B \to D^*\tau\nu$ and $B \to \tau\nu$ in a 2HDM of type III, Phys. Rev. D **86**, 054014 (2012).

[27] A. Datta, M. Duraisamy, and D. Ghosh, Diagnosing new physics in $b \to c\tau\nu_\tau$ decays in the light of the recent *BABAR* result, Phys. Rev. D **86**, 034027 (2012).

[28] M. Duraisamy and A. Datta, The full $B \to D^*\tau^-\bar{\nu}_\tau$ angular distribution and CP violating triple products, J. High Energy Phys. 09 (2013) 059.

[29] M. Duraisamy, P. Sharma, and A. Datta, Azimuthal $B \to D^*\tau^-\bar{\nu}_\tau$ angular distribution with tensor operators, Phys. Rev. D **90**, 074013 (2014).

[30] B. Bhattacharya, A. Datta, D. London, and S. Shivashankara, Simultaneous explanation of the R_K and $R(D^{(*)})$ puzzles, Phys. Lett. B **742**, 370 (2015).

[31] B. Bhattacharya, A. Datta, J. P. Guévin, D. London, and R. Watanabe, Simultaneous explanation of the R_K and $R_{D^{(*)}}$ puzzles: A model analysis, J. High Energy Phys. 01 (2017) 015.

[32] P. Biancofiore, P. Colangelo, and F. De Fazio, Anomalous enhancement observed in $B \to D^{(*)}\tau\bar{\nu}_\tau$ decays, Phys. Rev. D **87**, 074010 (2013).

[33] A. Crivellin, Effects of right-handed charged currents on the determinations of $|V_{ub}|$ and $|V_{cb}|$, Phys. Rev. D **81**, 031301 (2010).

[34] A. Celis, M. Jung, X.-Q. Li, and A. Pich, Sensitivity to charged scalars in $B \to D^{(*)}\tau\nu_\tau$ and $B \to \tau\nu_\tau$ decays, J. High Energy Phys. 01 (2013) 054.

[35] X.-G. He and G. Valencia, B decays with τ leptons in nonuniversal left-right models, Phys. Rev. D **87**, 014014 (2013).

[36] R. Dutta, A. Bhol, and A. K. Giri, Effective theory approach to new physics in $b \to u$ and $b \to c$ leptonic and semileptonic decays, Phys. Rev. D **88**, 114023 (2013).

[37] M. Tanaka and R. Watanabe, New physics contributions in $B \to \pi\tau\bar{\nu}$ and $B \to \tau\bar{\nu}$, Prog. Theor. Phys. **2017**, 013B05 (2017).

[38] N. G. Deshpande and X. G. He, Consequences of R-parity violating interactions for anomalies in $\bar{B} \to D^{(*)}\tau\bar{\nu}$ and $b \to s\mu^+\mu^-$, Eur. Phys. J. C **77**, 134 (2017).

[39] X. Q. Li, Y. D. Yang, and X. Zhang, Revisiting the one leptoquark solution to the $R(D^{(*)})$ anomalies and its

phenomenological implications, J. High Energy Phys. 08 (2016) 054.
[40] D. Du, A. X. El-Khadra, S. Gottlieb, A. S. Kronfeld, J. Laiho, E. Lunghi, R. S. Van de Water, and R. Zhou, Phenomenology of semileptonic B-meson decays with form factors from lattice QCD, Phys. Rev. D **93**, 034005 (2016).
[41] F. U. Bernlochner, $B \to \pi\tau\bar{\nu}_\tau$ decay in the context of type II 2HDM, Phys. Rev. D **92**, 115019 (2015).
[42] A. Soffer, B-meson decays into final states with a tau lepton, Mod. Phys. Lett. A **29**, 1430007 (2014).
[43] M. Bordone, G. Isidori, and D. van Dyk, Impact of leptonic τ decays on the distribution of $B \to P\mu\bar{\nu}$ decays, Eur. Phys. J. C **76**, 360 (2016).
[44] D. Bardhan, P. Byakti, and D. Ghosh, A closer look at the R_D and R_{D^*} anomalies, J. High Energy Phys. 01 (2017) 125.
[45] A. K. Alok, D. Kumar, S. Kumbhakar, and S. U. Sankar, D^* polarization as a probe to discriminate new physics in $B \to D^*\tau\bar{\nu}$, Phys. Rev. D **95**, 115038 (2017).
[46] M. A. Ivanov, J. G. Körner, and C. T. Tran, Exclusive decays $B \to \ell^-\bar{\nu}$ and $B \to D^{(*)}\ell^-\bar{\nu}$ in the covariant quark model, Phys. Rev. D **92**, 114022 (2015).
[47] M. A. Ivanov, J. G. Körner, and C. T. Tran, Analyzing new physics in the decays $\bar{B}^0 \to D^{(*)}\tau^-\bar{\nu}_\tau$ with form factors obtained from the covariant quark model, Phys. Rev. D **94**, 094028 (2016).
[48] S. M. Boucenna, A. Celis, J. Fuentes-Martin, A. Vicente, and J. Virto, Non-Abelian gauge extensions for B-decay anomalies, Phys. Lett. B **760**, 214 (2016).
[49] S. M. Boucenna, A. Celis, J. Fuentes-Martin, A. Vicente, and J. Virto, Phenomenology of an $SU(2) \times SU(2) \times U(1)$ model with lepton-flavour non-universality, J. High Energy Phys. 12 (2016) 059.
[50] S. Nandi, S. K. Patra, and A. Soni, Correlating new physics signals in $B \to D^{(*)}\tau\nu_\tau$ with $B \to \tau\nu_\tau$, arXiv:1605.07191.
[51] R. Dutta and A. Bhol, $b \to (c,u)\tau\nu$ leptonic and semileptonic decays within an effective field theory approach, Phys. Rev. D **96**, 036012 (2017).
[52] R. Alonso, B. Grinstein, and J. Martin Camalich, Lifetime of the B_c^- Mesons Constrains Explanations for Anomalies in $B \to D^{(*)}\tau\nu$, Phys. Rev. Lett. **118**, 081802 (2017).
[53] D. Bečirevič, S. Fajfer, N. Košnik, and O. Sumensari, Leptoquark model to explain the B-physics anomalies, R_K and R_D, Phys. Rev. D **94**, 115021 (2016).
[54] A. Celis, M. Jung, X. Q. Li, and A. Pich, Scalar contributions to $b \to c(u)\tau\nu$ transitions, Phys. Lett. B **771**, 168 (2017).
[55] F. Abe *et al.* (CDF Collaboration), Observation of B_c mesons in $p\bar{p}$ collisions at $\sqrt{s} = 1.8$ TeV, Phys. Rev. D **58**, 112004 (1998).
[56] I. P. Gouz, V. V. Kiselev, A. K. Likhoded, V. I. Romanovsky, and O. P. Yushchenko, Yad. Fiz. **67**, 1581 (2004) [Prospects for the B_c studies at LHCb, Phys. At. Nucl. **67**, 1559 (2004)].
[57] M. Pepe Altarelli and F. Teubert, B Physics at LHCb, Int. J. Mod. Phys. A **23**, 5117 (2008).
[58] I. I. Y. Bigi, Inclusive B_c decays as a QCD lab, Phys. Lett. B **371**, 105 (1996).
[59] M. Beneke and G. Buchalla, B_c meson lifetime, Phys. Rev. D **53**, 4991 (1996).
[60] C. H. Chang, S. L. Chen, T. F. Feng, and X. Q. Li, Lifetime of B_c meson and some relevant problems, Phys. Rev. D **64**, 014003 (2001).
[61] C. Patrignani *et al.* (Particle Data Group), Review of particle physics, Chin. Phys. C **40**, 100001 (2016).
[62] R. Aaij *et al.* (LHCb Collaboration), Measurement of the lifetime of the B_c^+ meson using the $B_c^+ \to J/\psi\pi^+$ decay mode, Phys. Lett. B **742**, 29 (2015).
[63] R. Aaij *et al.* (LHCb Collaboration), Measurement of the B_c^+ meson lifetime using $B_c^+ \to J/\psi\mu^+\nu_\mu X$ decays, Eur. Phys. J. C **74**, 2839 (2014).
[64] S. S. Gershtein, V. V. Kiselev, A. K. Likhoded, and A. V. Tkabladze, Usp. Fiz. Nauk **165**, 3 (1995) [Physics of B_c mesons, Phys. Usp. **38**, 1 (1995)].
[65] V. V. Kiselev, A. E. Kovalsky, and A. K. Likhoded, B_c decays and lifetime in QCD sum rules, Nucl. Phys. **B585**, 353 (2000).
[66] R. Dhir and R. C. Verma, B_c meson form factors and $B_c \to PV$ decays involving flavor dependence of transverse quark momentum, Phys. Rev. D **79**, 034004 (2009).
[67] E. Hernandez, J. Nieves, and J. M. Verde-Velasco, Study of exclusive semileptonic and non-leptonic decays of B_c^- in a nonrelativistic quark model, Phys. Rev. D **74**, 074008 (2006).
[68] M. A. Ivanov, J. G. Korner, and P. Santorelli, Semileptonic decays of the B_c meson, Phys. Rev. D **63**, 074010 (2001).
[69] M. A. Ivanov, J. G. Korner, and P. Santorelli, Semileptonic decays of B_c mesons into charmonium states in a relativistic quark model, Phys. Rev. D **71**, 094006 (2005); Erratum: Semileptonic decays of B_c mesons into charmonium states in a relativistic quark model, Phys. Rev. D **75**, 019901 (2007).
[70] M. A. Ivanov, J. G. Korner, and P. Santorelli, Exclusive semileptonic and nonleptonic decays of the B_c meson, Phys. Rev. D **73**, 054024 (2006).
[71] D. Ebert, R. N. Faustov, and V. O. Galkin, Properties of heavy quarkonia and B_c mesons in the relativistic quark model, Phys. Rev. D **67**, 014027 (2003).
[72] D. Ebert, R. N. Faustov, and V. O. Galkin, Weak decays of the B_c meson to charmonium and D mesons in the relativistic quark model, Phys. Rev. D **68**, 094020 (2003).
[73] D. Ebert, R. N. Faustov, and V. O. Galkin, Weak decays of the B_c meson to B_s and B mesons in the relativistic quark model, Eur. Phys. J. C **32**, 29 (2003).
[74] D. s. Du and Z. Wang, Predictions of the standard model for $B_c^\pm$ weak decays, Phys. Rev. D **39**, 1342 (1989).
[75] C. H. Chang and Y. Q. Chen, Decays of B_c meson, Phys. Rev. D **49**, 3399 (1994).
[76] J. F. Liu and K. T. Chao, B_c meson weak decays and CP violation, Phys. Rev. D **56**, 4133 (1997).
[77] A. Abd El-Hady, J. H. Munoz, and J. P. Vary, Semileptonic and nonleptonic B_c decays, Phys. Rev. D **62**, 014019 (2000).
[78] P. Colangelo and F. De Fazio, Using heavy quark spin symmetry in semileptonic B_c decays, Phys. Rev. D **61**, 034012 (2000).
[79] J. f. Sun, Y. l. Yang, W. j. Du, and H. l. Ma, Study of $B_c \to B^*P, BV$ decays with QCD Factorization, Phys. Rev. D **77**, 114004 (2008).

[80] W. Wang, Y. L. Shen, and C. D. Lu, Covariant fight-front approach for B_c transition form factors, Phys. Rev. D **79**, 054012 (2009).

[81] C. F. Qiao and R. L. Zhu, Estimation of semileptonic decays of B_c meson to S-wave charmonia with nonrelativistic QCD, Phys. Rev. D **87**, 014009 (2013).

[82] Z. J. Xiao and X. Liu, Study of the pure annihilation $B_c \to A_2 A_3$ decays, Phys. Rev. D **84**, 074033 (2011).

[83] X. Liu, Z. J. Xiao, and C. D. Lu, "The Pure annihilation type $B_c \to M_2 M_3$ decays in the perturbative QCD approach, Phys. Rev. D **81**, 014022 (2010).

[84] J. F. Cheng, D. S. Du, and C. D. Lu, Prediction of $B_c \to D\pi$ in the pQCD approach, Eur. Phys. J. C **45**, 711 (2006).

[85] J. F. Sun, D. S. Du, and Y. L. Yang, Study of $B_c \to J/\psi\pi$, $\eta_c\pi$ decays with perturbative QCD approach, Eur. Phys. J. C **60**, 107 (2009).

[86] W. F. Wang, Y. Y. Fan, and Z. J. Xiao, Semileptonic decays $B_c \to (\eta_c, J/\Psi) l\nu$ in the perturbative QCD approach, Chin. Phys. C **37**, 093102 (2013).

[87] K. K. Pathak and D. K. Choudhury, Semileptonic decay of B_c meson into $c\bar{c}$ states in a QCD potential model, Int. J. Mod. Phys. A **28**, 1350097 (2013).

[88] Y. K. Hsiao and C. Q. Geng, Branching fractions of $B_{(c)}$ decays involving J/ψ and $X(3872)$ Chin. Phys. C **41**, 013101 (2017).

[89] Z. Rui, H. Li, G. x. Wang, and Y. Xiao, Semileptonic decays of B_c meson to S-wave charmonium states in the perturbative QCD approach, Eur. Phys. J. C **76**, 564 (2016).

[90] R. Aaij *et al.* (LHCb Collaboration), Measurement of the ratio of B_c^+ branching fractions to $J/\psi\pi^+$ and $J/\psi\mu^+\nu_\mu$, Phys. Rev. D **90**, 032009 (2014).

[91] T. Bhattacharya, V. Cirigliano, S. D. Cohen, A. Filipuzzi, M. Gonzalez-Alonso, M. L. Graesser, R. Gupta, and H.-W. Lin, Probing novel scalar and tensor interactions from (ultra)cold neutrons to the LHC, Phys. Rev. D **85**, 054512 (2012).

[92] V. Cirigliano, J. Jenkins, and M. Gonzalez-Alonso, Semileptonic decays of light quarks beyond the standard model, Nucl. Phys. **B830**, 95 (2010).

[93] J. G. Korner and G. A. Schuler, Exclusive semileptonic heavy meson decays including lepton mass effects, Z. Phys. C **46**, 93 (1990).

[94] A. Kadeer, J. G. Korner, and U. Moosbrugger, Helicity analysis of semileptonic hyperon decays including lepton mass effects, Eur. Phys. J. C **59**, 27 (2009).

[95] B. Colquhoun, C. T. H. Davies, J. Kettle, J. Koponen, A. T. Lytle, R. J. Dowdall, and G. P. Lepage (HPQCD Collaboration), B-meson decay constants: A more complete picture from full lattice QCD, Phys. Rev. D **91**, 114509 (2015).

[96] A. Lytle, B. Colquhoun, C. Davies, J. Koponen, and C. McNeile, Semileptonic B_c decays from full lattice QCD, *Proc. Sci.*, BEAUTY2016 (2016) 069 [arXiv:1605.05645].

[97] D. Milanes, N. Quintero, and C. E. Vera, Sensitivity to Majorana neutrinos in $\Delta L = 2$ decays of B_c meson at LHCb, Phys. Rev. D **93**, 094026 (2016).

[98] R. Aaij *et al.* (LHCb Collaboration), Measurements of B_c^+ Production and Mass with the $B_c^+ \to J/\psi\pi^+$ Decay, Phys. Rev. Lett. **109**, 232001 (2012).

[99] R. Aaij *et al.* (LHCb Collaboration), Test of lepton universality with $B^0 \to K^{*0}\ell^+\ell^-$ decays, J. High Energy Phys. 08 (2017) 055.